A Rogers-Shephard Type Inequality for Surface Area

Fadia Ounissi

A Thesis

in The Department of

Mathematics and Statistics

Presented in Partial Fulfillment of the Requirements

For the Degree of Master of

Science (Mathematics)

at Concordia University

Montreal, Quebec, Canada

March 2024

CONCORDIA UNIVERSITY

SCHOOL OF GRADUATE STUDIES

This is to certify that the thesis prepared

By: Fadia Ounissi

Entitled: A Rogers-Shephard Type Inequality for Surface Area

and submitted in partial fulfillment of the requirements for the degree of

Master of Science (Mathematics)

complies with the regulations of the University and meets the accepted standards with respect to originality and quality.

Signed by the final examining committee:

_____ Chair and Examiner
Dr. Pawel Gora

_____ Examiner
Dr. Ronald Stern

_____ Supervisor
Dr. Alina Stancu

Approved by

_____
Dr. Lea Popovic, Graduate Program Director

_____ 2024

_____
Dr. Pascale Sicotte, Dean of Faculty of Arts and Science

ABSTRACT

A Rogers-Shephard Type Inequality for Surface Area

Fadia Ounissi

The famous Rogers-Shephard inequality states that, for any convex body $K \subset \mathbb{R}^n$, we have a volumetric inequality $V_n(K-K) \leq \binom{2n}{n} V_n(K)$ that compares the volume of the difference body of K, $K-K$, with the volume of K. Using Cauchy's surface area formula, a particular case of the more general *Kubota's Formulae for Quermassintegrals*, we extend this classical inequality to extrapolate an upper bound $C_K = \frac{S(K-K)}{S(K)}$ for the surface area of the difference body within the Euclidean space $\mathbb{R}^n$. We accompany this upper bound with a lower bound that we derive from the classical Brunn-Minkowski inequality, $V_n(A+B)^{1/n} \geq V_n(A)^{1/n} + V_n(B)^{1/n}$. Embracing a geometric perspective, we delve into the nuanced relationships between convex bodies and their respective surface areas, scrutinizing the patterns and properties of the difference body. This includes the validation of the upper bound in $\mathbb{R}^3$ for certain classes of convex bodies, including smooth bodies and polytopes. We then analyse and establish a pattern for the formation of the difference body of pyramidal structures in $\mathbb{R}^3$. Finally, we draw a conclusion on the effect of symmetry on C_K's proximity to either bound. More specifically, we observe how deviations from symmetry, mainly when K is a simplex, often considered the most asymmetric convex body, draws the constant closer to the upper bound.

Acknowledgments

I extend my deepest gratitude to Dr. Alina Stancu, whose unwavering belief in my potential has been a constant source of inspiration. Dr. Stancu not only introduced me to the world of geometry, but also fostered a learning environment that was both positive and enriching. Her passion and analytical prowess have left a mark on my academic journey. Working under her guidance has been a privilege, and I am proud to consider her not just a mentor but a source of continual motivation. Our routine interactions have been a testament to her dedication to my growth, and I will remember working under her supervision with fondness.

I would also like to express my sincere appreciation to the friends I made along the way, and I am grateful for the camaraderie we shared during this journey.

Lastly, I extend heartfelt thanks to my father. Despite not being familiar with my research, his consistent inquiries about the progress of my thesis have been a constant reminder of his unwavering support. I am delighted to share that the journey is now complete, and this completion marks not just an academic achievement, but a testament to the strength of the support system that surrounds me.

Contents

List of Figures

List of Tables

Chapter 1

Introduction and prerequisites

Convex geometry is a branch of geometry studying convex sets, mainly in the Euclidean space, which occur naturally in various other areas of mathematics, such as functional analysis, convex analysis, probability theory, optimization, and others. Although it is a relatively young mathematical discipline, it has seen immense growth at the turn of the 20^{th} century, mainly due to the known mathematicians Brunn and Minkowski.

Before jumping into the desired inequalities pertaining to this thesis, the first chapter serves to introduce some basic notions in convexity, mainly the necessary prerequisites used in our study such as convex sets, convex functions, Minkowski sums, and mixed volumes. We also revisit the classical Rogers-Shephard inequality for the difference body, which turns out to be quintessential for the extrapolation of the upper bound for the surface area of the difference body.

In the second chapter, we present an upper bound for the surface area of the difference body, using both Cauchy's surface area formula, a specific case of *Kubota's Formulae for Quermassintegrals*, and the Rogers-Shephard inequality. The main objective is to provide a proof supporting the claim that this upper bound can never be reached for any convex body $K \subset \mathbb{R}^n$.

Finally, in the subsequent chapter, we present numerical results for the upper bound for certain classes of convex bodies in $\mathbb{R}^3$, supported by Python codes that allows us to observe the formation of the difference body $K - K$. This will serve to describe how the difference body is formed, and provide a geometric interpretation for its construction that is combinatorial in nature.

1.1 Basic convexity

1.1.1 Convex sets

Throughout this thesis, we remain in the Euclidean space $\mathbb{R}^n$.

Definition 1.1.1 A set $A \subseteq \mathbb{R}^n$ is called a *convex set* if the line segment joining any two distinct points in the set A lies in A, i.e, $\forall \lambda \in [0,1]$ and $\forall x, y \in A$, $\lambda x + (1-\lambda y) \in A$.

This idea can be generalized to more than two points. In fact, a point of the form $\lambda_1 x_1 + \lambda_2 x_2 + \cdots + \lambda_m x_m$, where each $\lambda_i \geq 0$, and $\sum_{i=1}^m \lambda_i = 1$, is called a convex combination of the points $x_1, x_2, \cdots, x_m$. Clearly, every point in a convex set an be written as a convex combination of other points in the set, which implies that a set is convex if and only if it contains all convex combinations of its points.

This leads to an important definition in convexity:

Definition 1.1.2 The *convex hull* of a set A, commonly denoted by conv A, or conv(A) is the set of all convex combinations of points in A. That is:

$$\text{conv}(A) = \left\{ \sum_{i=1}^m \lambda_i x_i : \forall i = 1, ..., m, x_i \in A, \lambda_i \geq 0, \text{and } \sum_{i=1}^m \lambda_i = 1 \right\}.$$

The convex hull of a set A is also the smallest convex set containing A. In other words, for any convex set $B \subseteq \mathbb{R}^n$, if $A \subseteq B$, then conv $A \subseteq B$. Hence, conv A is the intersection of all convex sets containing A.

The convex hull of any set $A \subseteq \mathbb{R}^n$ is itself convex, and if A is convex, then conv $(A) = A$.

When dealing with compact convex sets, for any non-empty convex compact set $C \subset \mathbb{R}^n$, the set C is the convex hull of its *extreme points*, which are points in C not contained in the interior of any segment in C. In other words, if x is an extreme point, it cannot be written as $x = \lambda y + (1-\lambda)z$ for some $y, z \in C$ and some $\lambda \in (0,1)$. Hence, such extreme points are on the boundary of C, but not all boundary points are necessarily extreme points.

Since we will be dealing with polytopes, it is important to mention a consequence of the previous definition:

Definition 1.1.3 A polytope $P \subset \mathbb{R}^n$ is the convex hull of a finite set of points. Equivalently, it is also the convex hull of all of its extreme points, i.e., $P = \text{conv}\{x_i\}_{i=1}^m$ for some $m \in \mathbb{N}$. The extreme points of P are its vertices.

A second type of convex set we deal with is the *convex body*.

Definition 1.1.4 A *convex body* is a set $K \subseteq \mathbb{R}^n$ which is convex, compact, and has non-empty interior.

Note that the assumption on the non-empty interior implies that a convex body in $\mathbb{R}^n$ has strictly positive volume, i.e. n-dimensional Lebesgue measure. Clearly, this definition also implies that a polytope is also a convex body as long as it has non-empty interior.

Further on, we will see that extreme cases in various geometric inequalities for convex bodies often manifest when the convex body K is either *centrally symmetric* or a *simplex*. We will now proceed to formally define both:

Definition 1.1.5 A convex body $K \in \mathbb{R}^n$ is *centrally symmetric* if $K = -K$.

Definition 1.1.6 A *simplex* in $\mathbb{R}^n$, usually referred to as the *n-simplex*, is the simplest non-degenerate polytope in its respective dimension or the polytope with non-empty interior that has least number of vertices. In other words, an *n-simplex* contains $(n+1)-$vertices and $(n+1)-$faces, which are $(n-1)-$ dimensional simplices.

This definition will be crucial in encapsulating the fundamental characteristics of a simplex, and sets the stage for understanding its role in extreme cases of geometric inequalities for convex bodies in terms of volume and surface area, two cases that we will study in this thesis.

1.1.2 Convex functions

Definition 1.1.7 A function $f : \mathbb{R}^n \to (-\infty, +\infty]$ is convex if and only if

$$f(\lambda x + (1-\lambda)y) \leq \lambda f(x) + (1-\lambda)f(y),$$

$\forall x, y \in \mathbb{R}^n$, and $\forall \lambda \in [0,1]$.

Convex sets and convex functions are closely related. Indeed, a function $f : A \subset \mathbb{R}^n \to (-\infty, +\infty]$ with A convex is a convex function if it satisfies the same inequality, but note the requirement that the domain of the function must be a convex set.

We can also relate convex sets to convex functions through the *epigraph*.

Definition 1.1.8 The epigraph of a function f is the set

$$epi(f) = \{(x,t) \in \mathbb{R}^{n+1} : f(x) \leq t\}.$$

It is easy to see that f is a convex function if and only if its epigraph is a convex subset of $\mathbb{R}^{n+1}$.

1.1.3 Hyperplanes

Definition 1.1.9 A hyperplane h in $\mathbb{R}^n$ is a set of the form

$$h = h(u, \alpha) = \{v \in \mathbb{R}^n : \langle u, v\rangle = \alpha\},$$

where u is a fixed nonzero vector in $\mathbb{S}^{n-1}$, $\alpha \in \mathbb{R}$, and $\langle \cdot, \cdot \rangle$ is the Euclidean inner product of $\mathbb{R}^n$. It follows that a hyperplane $h(u, \alpha)$ defines two closed half-spaces:

$$h^+ = h^+(u, \alpha) = \{v \in \mathbb{R}^n : \langle u, v\rangle \geq \alpha\}$$
$$h^- = h^-(u, \alpha) = \{v \in \mathbb{R}^n : \langle u, v\rangle \leq \alpha\}.$$

In this thesis, we are interested in a specific type of hyperplanes, called *support* hyperplanes, that allows us to define convex bodies.

Definition 1.1.10 A hyperplane in $\mathbb{R}^n$ is called a *support* hyperplane of a given set A if A is contained entirely in one of the two closed half-spaces bounded by the hyperplane, and $A \cap h \neq \emptyset$. If $A \cap h = z$, then $z \in \partial A$ and we say that h supports A at z.

Definition 1.1.11 The *support function* of a compact convex set $K \subset \mathbb{R}^n$ is the function $h_k : \mathbb{S}^{n-1} \to \mathbb{R}$ defined by

$$h_K(u) = h(K, u) = \max\{\langle x, u\rangle \;\; x \in K\}$$

for each unit vector $u \in \mathbb{S}^{n-1}$. As such, the support function gives the signed distance from the origin to the support hyperplane of K of outer normal u. Conversely, we can define the support hyperplane for K at a point of its boundary $x \in \partial K$ by

$$H_u = \{x \in \mathbb{R}^n : \langle x, u\rangle = h_K(u)\}.$$

Recall from Definition 1.1.4 that a convex body $K \subset \mathbb{R}^n$ is convex, compact set of $\mathbb{R}^n$ with non-empty interior. The previous definitions are useful to describe the following geometric quantity for convex bodies:

Definition 1.1.12 Let $K \subset \mathbb{R}^n$ be a convex body. Then for each $u \in \mathbb{S}^{n-1}$,

$$w_K(u) = h_K(u) + h_K(-u)$$

is called the *width* of K in the direction of u, and represents the distance between the two supporting hyperplanes of K orthogonal to u.

Definition 1.1.13 Let $K \subset \mathbb{R}^n$ be a convex body containing the origin. Then its gauge function γ_K is given by:

$$\gamma_K(x) := \|x\|_K := \inf\{\lambda > 0 : x \in \lambda K\}.$$

1.1.4 Minkowski addition

The main component of this thesis relates to the concept of *Minkowski sum* or *vector sum* of sets, which we will now proceed to define.

Definition 1.1.14 Let $A, B \subseteq \mathbb{R}^n$ be non-empty sets. The *Minkowski sum of A and B* is defined as

$$A + B = \{a + b : a \in A, b \in B\}.$$

Further, we can also define a *Minkowski combination* of sets, which is a Minkowski sum of the form $\lambda_1 A_1 + \cdots + \lambda_m A_m$ for $A_1, \cdots, A_m \subseteq \mathbb{R}^n$, and $\lambda_1, \cdots, \lambda_m \geq 0$, where λA represents

$$\lambda A = \{\lambda a : a \in A, \lambda \geq 0\}.$$

Note that the sets need not be convex or compact for Minkowski addition or multiplication of a set by a scalar (often equivalent to scaling the set) to be defined. It is solely the vector space structure of $\mathbb{R}^n$ over the real numbers which is used here. Multiplication by a negative scalar can also be considered in the sense that -1 reflects the set K about the origin to obtain $-K$.

1.1.5 The Brunn-Minkowski inequality

The Brunn-Minkowski inequality comes in a few different, but ultimately related, versions.

Theorem 1.1.1 (First version). Let $A, B \subseteq \mathbb{R}^n$ be compact non-empty sets, and let $\lambda \in (0,1)$. Then

$$V_n(\lambda A + (1-\lambda)B) \geq V_n(A)^{\lambda} V_n(B)^{1-\lambda}.$$

Although this is the first version of this quintessential theorem, the second and third versions are also widely used in convexity:

Corollary 1.1.2 (Brunn-Minkowski inequality, second version). Let $A, B \subseteq \mathbb{R}^n$ be compact non-empty sets. Then

$$V_n(A+B)^{1/n} \geq V_n(A)^{1/n} + V_n(B)^{1/n}.$$

Using a small modification of the previous corollary, and applying the inequality to the sets λA and $(1-\lambda)B$, we obtain the third version:

Corollary 1.1.3 (Brunn-Minkowski inequality, third version). Let $A, B \subseteq \mathbb{R}^n$ be compact non-empty sets. Then

$$V_n(\lambda A + (1-\lambda)B)^{1/n} \geq \lambda V_n(A)^{1/n} + (1-\lambda) V_n(B)^{1/n} \tag{1.1}$$

for all $\lambda \in (0,1)$.

The three inequalities were proven to be equivalent, and the third version shows that the n^{th} root of the n-dimensional volume of compact non-empty sets of $\mathbb{R}^n$ is a concave function on the space of compact sets in $\mathbb{R}^n$.

As for the equality case, it can be proven that it holds for some $\lambda \in (0,1)$ if and only if A and B are *homothetic*, i.e. $\exists x \in \mathbb{R}^n$ and a non-negative real scalar $\lambda \geq 0$ such that $A = x + \lambda B$.

1.1.6 Mixed volumes

Given a collection of convex bodies, mixed volumes are a concept that provides a way to measure their combined size or volume. In fact, the volume of a Minkowski combination of m compact convex sets is a polynomial of degree n whose coefficients are called mixed volumes, as stated in the following theorem:

Theorem 1.1.4 Let $K_1, K_2, \ldots, K_m$ be a family of compact convex sets in $\mathbb{R}^n$. Then, there exist coefficients $V(K_{j_1}, K_{j_2}, \ldots, K_{j_n}), 1 \leq j_1, \ldots, j_n \leq m$, symmetric in the indices, such that

$$V_n(\lambda_1 K_1 + \cdots + \lambda_m K_m) = \sum_{j_1,\ldots,j_n=1}^{m} V(K_{j_1}, K_{j_2}, \ldots, K_{j_n})\lambda_{j_1} \ldots \lambda_{j_n},$$

where, for each $i = 1, \ldots, n$, $j_i \in \{1, 2, \ldots, m\}$ and $V_n(\lambda_1 K_1 + \cdots + \lambda_m K_m)$ is a homogeneous polynomial of degree n in $(\lambda_1, \ldots, \lambda_m)$. The coefficients $V(K_{j_1}, K_{j_2}, \ldots, K_{j_n})$ are called *mixed volumes*.

This implies that $V_n(\lambda K) = \lambda^n V_n(K) = V(K, \ldots, K)\lambda^n$, where the mixed volume $V(K, \ldots, K)$ is the volume of K. A simple application of the above theorem to $V_n(K + \epsilon B^n)$, where B^n is the unit ball in $\mathbb{R}^n$, yields that

$$V(K + \epsilon B^n) = W_0(K) + \binom{n}{1} W_1(K)\lambda + \ldots + \binom{n}{n} W_n(K)\lambda^n,$$

where the coefficients $W_i(K) = V(\underbrace{K, \ldots, K}_{n-i}, \underbrace{B^n, \ldots, B^n}_{i}),\ 0 \leq i \leq n$, are called the *quermassintegrals* of K. This leads to the following definition:

Definition 1.1.15 Minkowski's surface area $S(K)$ for a nonempty compact convex set K in $\mathbb{R}^n$ is given by

$$S(K) = \lim_{\epsilon \searrow 0} \frac{V(K + \epsilon B^n) - V(K)}{\epsilon} = nW_1(K) = nV(K, \ldots, K, B^n).$$

For notation purposes, from now on, we will denote the volume of a convex body K by $V_n(K)$, and its surface area by $S(K)$.

Finally, f more details and applications of the previous definitions, we refer the reader to the book by Gruber [6], or the book by Balestro [2].

1.1.7 Curvature

The study of the upper bound $C_K = \frac{S(K-K)}{S(K)}$ mentioned in the abstract requires the usage of some concepts from differential geometry, notably the notions of the *Gauss map* and that of *curvature*.

Definition 1.1.16 For any smooth convex body K, we can define the *Gauss map* $\mathcal{G} : \partial K \to \mathbb{S}^{n-1}$ as the continuous map that associates to each point $p \in \partial K$ the unique outer normal unit vector $u \in \mathbb{S}^{n-1}$ of K at p.

Definition 1.1.17 For any smooth, convex body K whose boundary is twice differentiable, we define the inverse Gauss map as $\gamma : \mathbb{S}^{n-1} \to \partial K$. Then, the derivative of this map,

$$d\gamma|_u : u^\perp \to u^\perp,$$

where $u^\perp$ is the linear subspace of $\mathbb{R}^n$ orthogonal to u, is a linear endomorphism known as the *inverse Weingarten map*.

Definition 1.1.18 Let the inverse Gauss map be $\gamma : \mathbb{S}^{n-1} \to \partial K$ for any smooth, convex body K whose boundary is twice differentiable. Then, the *Gaussian curvature* $\kappa_K(p)$ of ∂K at p is given by

$$\kappa_K(p) = \frac{1}{Det(d\gamma|_u)} \in \mathbb{R}.$$

Definition 1.1.19 For a convex body in $\mathbb{R}^3$, the principal radii of curvature of its boundary ρ_1 and ρ_2 at the point $p = \gamma(u)$ are determined by considering all possible

unit vectors w that are orthogonal to u, thus tangent to the boundary of the body, and the curves with tangent vector w. The maximum value among the radii of curvature of these normal curves determines the minimum curvature $k_1 = \frac{1}{\rho_1}$, and the minimum value determines the maximum curvature $k_2 = \frac{1}{\rho_2}$. The principal curvatures are these extreme values

$$k_1 = \min_w k_w$$

$$k_2 = \max_w k_w.$$

Furthermore, the curvature of ∂K at $p = \gamma(u)$ is the product of the inverses of the principal radii of curvature. In other words, the *Gaussian curvature* of ∂K at p is the product of the principal curvatures, i.e.,

$$\kappa_K(p) = \frac{1}{Det(d\gamma|_u)} = k_1 k_2.$$

Generally, the principal curvatures are the eigenvalues of the Weingarten map which addresses the higher dimensional case. Each principal curvature is the curvature of a *normal* curve tangent to a principal direction. The principal directions form a basis of the tangent plane to the boundary of K at the point p of outer normal u.

For more information on curvature using this set-up, we refer to the book by Martini et al. [7], otherwise, for more general definitions or alternative descriptions, to any textbook on the differential geometry of hypersurfaces in Euclidean space.

1.2 Volume of the difference body

In the preceding sections, we established foundational insights into the geometric properties and definitions of convexity. We now turn our attention to a pivotal inequality in convex geometry known as the Rogers-Shephard inequality. The Rogers-

Shephard inequality provides a crucial understanding of the relationship between the volume of convex bodies and their symmetrals given by the Minkowski sum of the body with its reflection, laying the groundwork for further exploration into surface area inequalities, or generally inequalities for quermassintegrals of such symmetrals.

Before delving into our exploration of surface area inequalities, let us first revisit and present the proof for the Rogers-Shephard inequality. This inequality, attributed to Rogers and Shephard [9], serves as a cornerstone for subsequent analysis.

Definition 1.2.1 Let $K \in \mathbb{R}^n$ be a convex body. Then

$$K - K = K + (-K) = \{x - y \in \mathbb{R}^n : x, y \in K\} = \{x + (-y) : x, y \in K\}$$

is called the *difference body of* K, where $K - K$ is the Minkowski sum of the convex body K in $\mathbb{R}^n$ with its reflection about the origin, $-K$.

A simple application of the Brunn-Minkowski inequality to the volume of the difference body $V_n(K-K)$ yields a lower bound for its volume in terms of $V_n(K)$. Using $V_n(K) = V_n(-K)$, we get

$$\begin{aligned} V_n(K - K) &\geq (V_n(K)^{1/n} + V_n(-K)^{1/n})^n \\ &= (V_n(K)^{1/n} + V_n(K)^{1/n})^n \\ &= (2V_n(K)^{1/n})^n \\ &= 2^n V_n(K), \end{aligned} \tag{1.2}$$

where the equality holds if and only if K is centrally symmetric.

Theorem 1.2.1 [9] (The Rogers-Shephard inequality): Let $K \in \mathbb{R}^n$ be a convex body. Then

$$V_n(K-K) \leq \binom{2n}{n} V_n(K) \tag{1.3}$$

with equality if and only if K is a simplex.

Before proceeding to prove this classical inequality, we will first introduce some definitions, and provide proofs that will be essential.

To start, a short proof shows that the next definition is equivalent to the difference body introduced in Definition 1.2.1:

$$K - K = \{x \in \mathbb{R}^n : K \cap (K + x) \neq \varnothing\}.$$

Proof. First, let $x \in K - K$. Then $\exists y, z \in K$ such that $x = y - z$. Then $y = x + z$ implies that $y \in (K \cap (K + x))$. Next, let $y \in K \cap (K + x)$. Then $\exists z \in K$ such that $y = z + x \in K$, from which we get that $x = y - z$. Hence, equivalence is shown. □

Lemma 1.2.1 The function $f : K - K \to [0, +\infty)$ defined by $f(x) = V_n(K \cap (K + x))^{1/n}$ is a concave function.

Proof. We can prove the lemma by using the following inclusion:

$\forall x, y \in K - K$, and $\forall \lambda \in [0, 1]$,

$$(1-\lambda)(K \cap (K + x)) + \lambda(K \cap (K + y)) \subseteq K \cap (K + (1-\lambda)x + \lambda y).$$

(i) Let $z \in K \cap (K + x)$, $w \in K \cap (K + y)$. Since $z, w \in K$, then by convexity of K, $(1-\lambda)z + \lambda w \in K$. Hence,

$$(1-\lambda)(K \cap (K + x)) + \lambda(K \cap (K + y)) \subseteq K.$$

(ii) Let $z = x + x_0$, $w = y + y_0$, $x_0, y_0 \in K$. Then:

$$\begin{aligned}(1-\lambda)z + \lambda y &= (1-\lambda)(x+x_0) + \lambda(y+y_0)\\ &= (1-\lambda)x + \lambda y + (1-\lambda)x_0 + \lambda y_0\\ &\subseteq (1-\lambda)x + \lambda y + K.\end{aligned}$$

Therefore, $(1-\lambda)z+\lambda y = (1-\lambda)(x+x_0)+\lambda(y+y_0) \subseteq (1-\lambda)x + \lambda y + K$. Then, by using the Brunn-Minkowski inequality in (1.1),

$$\begin{aligned}V_n(K \cap (K + (1-\lambda)x + \lambda y))^{1/n} &\geq V_n((1-\lambda)(K \cap (K+x)) + \lambda(K \cap (K+y)))^{1/n}\\ &\geq V_n((1-\lambda)(K \cap (K+x)))^{1/n} + V_n(\lambda(K \cap (K+y)))^{1/n}\\ &= (1-\lambda)V_n(K \cap (K+x))^{1/n} + \lambda V_n(K \cap (K+y))^{1/n}.\end{aligned}$$

This shows that the function $f(x) = V_n(K \cap (K+x))^{1/n}$ is concave. □

Now, we define one last function required to prove Theorem 1.2.1. Let $g : K - K \to \mathbb{R}^n$ such that $\forall x \in K - K$ as a function on the unit sphere, we can write x as $x = r\theta$, $\theta \in S^{n-1}$, and $0 \leq r \leq \rho_{K-K}(\theta)$. Here, ρ_{K-K} is the radial function of $K - K$, where

$$\rho_{K-K}(\theta) = \max\{t > 0 : t\theta \in K - K\}.$$

This implies that there exists a unique scalar $\rho_{K-K}(\theta)$ such that the vector $\rho_{K-K}(\theta)\,\theta \in \partial(K-K)$. Then, $g(x) = f(0)\left(1 - \frac{r}{\rho_{K-K}(\theta)}\right)$, $0 \leq \frac{r}{\rho_{K-K}(\theta)} \leq 1$, is a linear function that vanishes on the boundary of the difference body $K - K$, and $g(0) = f(0)$. Since $f(x)$ is concave, $f(x) \geq g(x)$ on $K - K$.

Using the gathered necessary definitions, we now move to the proof of Theorem 1.2.1.

Proof. (Theorem 1.2.1): Let $K \in \mathbb{R}^n$ be a convex body. Then:

$$\int_{K-K} V_n(K \cap (K+x))dx = \int_{K-K} f(x)^n dx \geq \int_{K-K} g(x)^n dx.$$

The next part requires changing from Cartesian to polar coordinates. If σ is the rotationally invariant metric on the unit sphere S^{n-1} induced by the Euclidean structure, and the surface area of the sphere $\mathbb{S}^{n-1}$ is $\omega_n = n\kappa_n$, with κ_n the volume of the unit ball $\mathbb{B}^n$ in $\mathbb{R}^n$, we proceed as follows:

$$\begin{aligned}
\int_{K-K} g(x)^n dx &= \int_{S^{n-1}} \int_0^{\rho_{K-K}(\theta)} f(0)^n \left(1 - \frac{r}{\rho_{K-K}(\theta)}\right) r^{n-1} \frac{2\pi^{n/2}}{\Gamma(n/2)} dr d\sigma(\theta) \\
&= \omega_n f(0)^n \int_{S^{n-1}} \int_0^{\rho_{K-K}(\theta)} \left(1 - \frac{r}{\rho_{K-K}(\theta)}\right) r^{n-1} dr d\sigma(\theta) \\
&= n\kappa_n V_n(K) \int_{S^{n-1}} \int_0^1 (1-t)^n t^{n-1} \rho_{K-K}^n(\theta) d\sigma(\theta) dt \\
&= n\kappa_n V_n(K) \int_{S^{n-1}} \rho_{K-K}^n(\theta) d\sigma(\theta) \int_0^1 (1-t)^n t^{n-1} dt,
\end{aligned}$$

where the last integral is simply the Beta function, which yields

$$= V_n(K) V_n(K-K) n \frac{\Gamma(n)\Gamma(n+1)}{\Gamma(2n+1)} = V_n(K-K) V_n(K) \binom{2n}{n}^{-1}.$$

On the other hand, using Fubini's Theorem, we get

$$\begin{aligned}
&\int_{K-K} V_n(K \cap (K+x))dx = \int_{\mathbb{R}^n} V_n(K \cap (K+x))dx \\
&= \int_{\mathbb{R}^n} \int_{\mathbb{R}^n} 1_{K \cap (K+x)}(y) dy dx = \int_{\mathbb{R}^n} \int_{\mathbb{R}^n} 1_K(y) 1_{x+K}(y) dy dx \\
&= \int_{\mathbb{R}^n} 1_K(y) \left(\int_{\mathbb{R}^n} 1_{y-K}(x) dx \right) dy = V_n(y-K) \int_{\mathbb{R}^n} 1_K(y) dy = V_n(K)^2.
\end{aligned}$$

Combining both parts, we conclude with

$$V_n(K)^2 \geq V_n(K)V_n(K-K)\binom{2n}{n}^{-1},$$

which yields the desired inequality in (1.3). □

Remark: As a consequence of using the Brunn-Minkowski inequality, the equality case holds only when $K \cap (K+x)$ and K are homothetic to each other $\forall x \in K-K$, which was proven to occur if and only if K is a simplex [9]. The following corollary is an interesting consequence of the Rogers-Shephard inequality.

Corollary 1.2.2 [9] Let $K, L \subset \mathbb{R}^n$ be convex bodies. Then

$$V_n(K-L) \leq \binom{2n}{n} V_n(K+L).$$

Proof. Indeed, by a simple inclusion, $(K-L) \subseteq (K-L)-(K-L) = (K+L)-(K+L)$, which, combined with Theorem 1.2.1, yields the following inequality:

$$V_n(K-L) \leq V_n((K+L)-(K+L)) \leq \binom{2n}{n} V_n(K+L).$$

□

For more insights on the Rogers-Shephard inequality, we refer to the original paper by Rogers and Shephard, [9].

Chapter 2

Bounds for the surface area of the difference body in $\mathbb{R}^n$

2.1 Cauchy's surface area formula

Before we proceed, we need to introduce *Cauchy's surface area formula*. The following theorem will be essential for our surface area bound in $\mathbb{R}^n$. The formula introduced here is a particular case of the more general *Kubota's Formulae for Quermassintegrals* [6, p. 108-109].

Theorem 2.1.1 [6]. Suppose $K \subset \mathbb{R}^n$ is a convex body. Then

$$S(K) = \frac{1}{\kappa_{n-1}} \int_{\mathbb{S}^{n-1}} vol_{n-1}(\text{proj}u^{\perp}(K)) d\mathcal{H}^{n-1}(u),$$

where $d\mathcal{H}^{n-1}(u)$ is the integration with respect to the Hausdorff $(n-1)$-dimensional measure on $\mathbb{S}^{n-1}$, and κ_{n-1} is the $(n-1)$-dimensional volume of the Euclidean unit ball $\mathbb{B}^{n-1}$ in $\mathbb{R}^{n-1}$.

2.2 The lower bound

Theorem 2.2.1 Suppose $K \subset \mathbb{R}^n$ is a convex body. Then

$$S(K-K) \geq 2^{n-1} S(K), \tag{2.1}$$

with equality if and only if K is symmetric about some point $x_0 \in Int\,(K)$.

Proof. To prove this inequality, we first apply Theorem 2.1.1 to the projection of $K-K$. Since $\mathrm{proj}u^{\perp}(A)$ of a convex body $A \in \mathbb{R}^n$ yields a convex body in $\mathbb{R}^{n-1}$, we can use the linearity of the projection operator to apply the inequality in (1.2) to a difference of convex bodies in $\mathbb{R}^{n-1}$:

$$\begin{aligned}
S(K-K) &= \frac{1}{\kappa_{n-1}} \int_{\mathbb{S}^{n-1}} vol_{n-1}(\mathrm{proj}u^{\perp}(K-K)) d\mathcal{H}^{n-1}(u) \\
&= \frac{1}{\kappa_{n-1}} \int_{\mathbb{S}^{n-1}} vol_{n-1}(\mathrm{proj}u^{\perp}(K) + \mathrm{proj}u^{\perp}(-K)) d\mathcal{H}^{n-1}(u) \\
&= \frac{1}{\kappa_{n-1}} \int_{\mathbb{S}^{n-1}} vol_{n-1}(\mathrm{proj}u^{\perp}(K) - \mathrm{proj}u^{\perp}(K)) d\mathcal{H}^{n-1}(u) \\
&\geq \frac{1}{\kappa_{n-1}} \int_{\mathbb{S}^{n-1}} 2^{n-1} vol_{n-1}(\mathrm{proj}u^{\perp}(K)) d\mathcal{H}^{n-1}(u) \\
&= 2^{n-1} \frac{1}{\kappa_{n-1}} \int_{\mathbb{S}^{n-1}} vol_{n-1}(\mathrm{proj}u^{\perp}(K)) d\mathcal{H}^{n-1}(u) \\
&= 2^{n-1} S(K).
\end{aligned}$$

This inequality is sharp. Indeed, if K is symmetric about some point x_0, i.e., $K - x_0 = -(K - x_0)$, then $-K = K - 2x_0$, and we obtain

$$S(K-K) = S(K + K - 2x_0) = S(2(K - x_0)) = 2^{n-1} S(K - x_0) = 2^{n-1} S(K),$$

where the last equality comes from the homogeneity of the surface area of compact sets, and the surface area's invariance under translation. The other direction follows

from the equality cases of the classical Rogers-Shephard inequality in dimension $n-1$ in all directions $u \in \mathbb{S}^{n-1}$, and the fact that K is centrally symmetric if all its $(n-1)$-dimensional projections are centrally symmetric, [3].

□

2.3 The upper bound

In this section, we prove that there exists an upper bound C_K for all convex bodies $K \subset \mathbb{R}^n$.

Theorem 2.3.1 Suppose $K \subset \mathbb{R}^n$ is a convex body. Then

$$S(K-K) \leq \binom{2(n-1)}{n-1} S(K). \tag{2.2}$$

Proof. Similarly to the proof of Theorem 2.2, we use Theorem 2.1.1 and the linearity of the projection operator to obtain the difference body for $\mathrm{proj}u^{\perp}(K)$. Now that we have an $(n-1)$-dimensional convex body, we can apply the Rogers-Shephard inequality (1.3):

$$\begin{aligned} S(K-K) &= \frac{1}{\kappa_{n-1}} \int_{\mathbb{S}^{n-1}} vol_{n-1}(\mathrm{proj}u^{\perp}(K-K)) d\mathcal{H}^{n-1}(u) \\ &= \frac{1}{\kappa_{n-1}} \int_{\mathbb{S}^{n-1}} vol_{n-1}(\mathrm{proj}u^{\perp}(K) - \mathrm{proj}u^{\perp}(K)) d\mathcal{H}^{n-1}(u) \\ &\leq \frac{1}{\kappa_{n-1}} \int_{\mathbb{S}^{n-1}} \binom{2(n-1)}{(n-1)} vol_{n-1}(\mathrm{proj}u^{\perp}(K)) d\mathcal{H}^{n-1}(u) \\ &= \binom{2(n-1)}{(n-1)} S(K). \end{aligned}$$

□

Although the equality case for the lower bound in (2.1) is attained when K is a symmetric convex body, the case for the upper bound is more nuanced. First,

equality is always reached when $n = 2$. Indeed, for any convex body $K \subset \mathbb{R}^2$, what we have denoted as $S(K)$ corresponds to $nW_1(K)$ or $nV(K \ldots, K, B^n)$ (see Definition 1.1.15). If $n = 2$, then $nW_1(K) = nW_{n-1}$. The formula for W_{n-1}, [10, p. 296-297], is given by:

$$W_{n-1}(K) = V(K, \ldots, K, B^n) = \frac{1}{n} \int_{\mathbb{S}^{n-1}} h_K(u) d\mathcal{H}^{n-1}(u),$$

which is linear with respect to Minkowski addition. Thus, for $n = 2$:

$$W_1(K) = V(K, B^2) = \frac{1}{2} \int_{\mathbb{S}^1} h_K(u) d\mathcal{H}(u).$$

Applying it to $K - K$, we obtain:

$$\begin{aligned} W_1(K-K) = V(K-K, B^2) =& \frac{1}{2} \int_{\mathbb{S}^1} h_{K-K}(u) d\mathcal{H}(u) \\ =& \frac{1}{2} \int_{\mathbb{S}^1} \left(h_K(u) + h_{-K}(u)\right) d\mathcal{H}(u) \\ =& \frac{1}{2} \int_0^{2\pi} \left(h_K(\theta) + h_{-K}(\theta)\right) d\theta. \end{aligned}$$

For a convex body K, we have that $h_{-K}(\theta) = h_K(\theta + \pi)$. Now, let $\omega = \theta + \pi$. Since $d\omega = d\theta$, the previous integral becomes:

$$\begin{aligned} =& \frac{1}{2} \int_0^{2\pi} \left(h_K(\theta) + h_{-K}(\theta)\right) d\theta \\ =& \frac{1}{2} \int_0^{2\pi} \left(h_K(\theta) + h_K(\theta + \pi)\right) d\theta \\ =& \frac{1}{2} \int_0^{2\pi} h_K(\theta) d\theta + \frac{1}{2} \int_0^{2\pi} h_K(\omega) d\omega \\ =& 2V(K, B^2) = 2W_1(K). \end{aligned}$$

Hence, $\frac{W_1(K-K)}{W_1(K)} = 2$, for all convex bodies, and we reach equality in Theorem

2.3.1.

For $n \geq 3$, then equality can occur in (2.2) for some convex body K if and only if $\text{proj}_{u^\perp}(K)$ is a simplex for any $u \in \mathbb{S}^{n-1}$ per the Rogers-Shephard inequality (1.3). We aim to support the conjecture that this situation cannot occur for any convex body $K \subset \mathbb{R}^n$ for any dimension $n \geq 3$.

This supporting argument will be divided in three parts; we will first prove that for any simplex $K \subset \mathbb{R}^n$, there exists a vector $u \in \mathbb{S}^{n-1}$ such that $\text{proj}_{u^\perp}(K)$ is not a simplex. Then, although the complete claim will remain unproven, we offer a preliminary rationale for polytopes in $\mathbb{R}^n$ described as the convex hull of $m > n+1$ vertices. Polytopes are convex bodies with a finite number of extreme points, while any other convex body has an infinite (uncountable) number of extreme points, some subset of which determines a strictly convex connected sub-region of the boundary. Recall that boundaries of convex bodies are of class $\mathcal{C}^2$ except for a set of measure zero with respect to the surface area measure [2]. Then, for any non-polytopal convex body, there exists a strictly convex sub-region of the boundary of class $\mathcal{C}^2_+$, where the plus sign stands for strictly positive curvature. Thus, lastly, we will use some concepts from differential geometry to prove the claim for any convex body whose boundary contains at least one strictly convex, connected region of class $\mathcal{C}^2_+$.

- K is a simplex.

  We will first present a hands-on proof for a simplex in $\mathbb{R}^3$.

  Assume that T is a regular simplex in $\mathbb{R}^3$ with vertices $A = (1,1,0), B = (0,0,0), C = (1,0,1)$, and $D = (0,1,1)$. We will show that there exists a vector $u \in \mathbb{S}^{n-1}$ such that $\text{proj}_{u^\perp}(T)$ is a quadrilateral. The facet formed by the $\text{conv}\{A,C,D\}$ has the following unit normal:

$$\vec{n}_1 = \tfrac{1}{\sqrt{3}}\langle 1,1,1\rangle.$$

Equivalently, the facet formed by $\text{conv}\{B, C, D\}$ has the following unit normal:

$$\vec{n}_2 = \tfrac{1}{\sqrt{3}}\langle -1, -1, 1\rangle.$$

We are now interested in projecting K onto the hyperplane containing the curve joining points C and D with unit normal $\vec{u} = \frac{1}{\|\vec{n}_1+\vec{n}_2\|}(\vec{n}_1 + \vec{n}_2) = \langle 0, 0, 1\rangle$. Then using the formula of the projection of a point onto a hyperplane with normal u,

$$\text{proj}u^{\perp}(x) = x - \langle x, u\rangle u,$$

we can find the projections of K's vertices:

$$\begin{aligned}
A' &= \text{proj}\vec{u}^{\perp}(A) = \text{proj}\vec{u}^{\perp}(1, 1, 0) = (1, 1, 0)\\
B' &= \text{proj}\vec{u}^{\perp}(B) = \text{proj}\vec{u}^{\perp}(0, 0, 0) = (0, 0, 0)\\
C' &= \text{proj}\vec{u}^{\perp}(C) = \text{proj}\vec{u}^{\perp}(1, 0, 1) = (1, 0, 0)\\
D' &= \text{proj}\vec{u}^{\perp}(D) = \text{proj}\vec{u}^{\perp}(0, 1, 1) = (0, 1, 0).
\end{aligned}$$

Clearly, these form a unit square on the hyperplane $z = 0$. This result can be generalized to any $n-$simplex $\in \mathbb{R}^n$. We will proceed to prove this in reverse by expanding on an argument informally given by Martin Winter [12], which first assumes the existence of a polytope with $n + 1$ vertices in $\mathbb{R}^{n-1}$.

Claim: For every simplex $S \subset \mathbb{R}^n$ (with $n + 1$ vertices), there exists a vector $u \in \mathbb{S}^{n-1}$ such that the orthogonal projection $\text{proj}_{u^{\perp}}(S)$ also has $n+1$ vertices. We will approach the proof of this claim slightly differently than above.

Consider a polytope $P \subset \mathbb{R}^{n-1}$ with $n+1$ vertices, denoted by $\{y_0, y_1, \ldots, y_n\} \in \mathbb{R}^{n-1}$. Define $n + 1$ vertices in $\mathbb{R}^n$ by adding an extra n-th coordinate as follows:

$$p_i = \begin{cases} (y_i, 0) & \text{for } i \leq n-1 \\ (y_i, 1) & \text{for } i = n. \end{cases}$$

These vertices define a simplex $S_P \subset \mathbb{R}^n$, and the orthogonal projection of S_P onto the first $n-1$ coordinates yields P. Since any two simplices in $\mathbb{R}^n$ are affinely equivalent, there exists an affine transformation $T : \mathbb{R}^n \to \mathbb{R}^n$ such that $TS_P = \bar{S}$ for any simplex $\bar{S} \subset \mathbb{R}^n$. Now, consider the cylinder $C = P + \mathbb{R}e_n$ in $\mathbb{R}^n$. The intersection of C with the subspace $\mathbb{R}^{n-1}$, denoted as $C \cap \mathbb{R}^{n-1}$, remains a polytope with $n+1$ vertices under the application of T.

This intersection $TC \cap T\mathbb{R}^{n-1}$ is affinely equivalent to the orthogonal projection $\text{proj}_{u^\perp}(S)$, where u is any unit vector in $\mathbb{R}^n$ with the last component equal to zero. Therefore, for any simplex $S \subset \mathbb{R}^n$, there exists a vector $u \in \mathbb{S}^{n-1}$ such that $\text{proj}_{u^\perp}(S)$ has $n+1$ vertices. This implies that this projection cannot be a simplex.

- K is a polytope with $m \geq n+2$ vertices.

  Consider the previous case where K is a simplex, i.e. the convex hull of $n+1$ vertices. As the number of vertices increases, it is intuitive to expect the projection to have at least the same number of extreme points/vertices. Recall the previously constructed simplex S_p with $n+1$ vertices $p_i,\ 0 \leq i \leq n$ and let us consider the effect of adding more points to this construction.

  Suppose we add k additional points $p_{n+1}, p_{n+2}, \cdots, p_{n+k}$ to S_p, with a similar construction, such that the new polytope in $\mathbb{R}^{n-1}$ is the convex hull of the following vertices:

$$p_i = \begin{cases} (y_i, 0) & \text{for } i \leq n-1 \\ (y_i, 1) & \text{for } i = n \\ (y_i, 0) & \text{for } n+1 \leq i \leq n+k. \end{cases}$$

By adding these vertices, we extend S_p's base, and the polytope $Q = \text{conv}\ \{p_i\}_{i=0}^{n+k}, k \geq 1$, is no longer a simplex. Then its projection onto the points $(y_i, 0)$, $0 \leq i \leq n+k, i \neq n$ yields a polytope $P' \subset \mathbb{R}^{n-1}$, which contains more than $n+1$ vertices, proving that adding more vertices to construct the polytope $Q \subset \mathbb{R}^n$ increases the number of extreme points in its orthogonal projection. Furthermore, this construction shows that we can embed a polytope $P' \subset \mathbb{R}^{n-1}$ and obtain a polytope $Q \subset \mathbb{R}^n$ with at least $n+1$ vertices in its orthogonal projection, provided ∂Q contains a region $P' \subset \{x_n = 0\}$ (or some plane $\{x_i = c\}, 1 \leq i \leq n, c \in \mathbb{R}$) defined as the convex hull of $m-1$ vertices. However, this argument does not rule out that there may exist a polytope with $m \geq n+2$ vertices with each $(n-1)$-projection being a simplex as it is not true that any two polytopes with m vertices are affine images of each other.

To conclude that for any convex polytope $K \subset \mathbb{R}^n$ with $m \geq n+2$ vertices there exists an $(n-1)$-projection with $n+1$ or more vertices, it becomes difficult to keep track of newly added vertices. For this reason, the proof remains incomplete.

- K's boundary contains at least one strictly convex, connected region.

  This implies that there exists a region of ∂K with infinitely many extreme points with positive Gauss curvature.

  Let p be a point in boundary of a convex body $K \subset \mathbb{R}^n$, and assume that ∂K is of class $\mathcal{C}_+^2$ at p. This also means that if we choose u to be a unit normal vector of K at p, then u is unique.

Let H be a normal 2-plane generated by unit vectors u and w, where w is a fixed tangent vector to ∂K at p. Assume $\Pi : \mathbb{R}^n \to H$ is the map for the orthogonal projection onto H, $\mathcal{G} : \partial K \to S^{n-1}$ is the Gauss map (see Definition 1.1.16), and $\gamma : S^{n-1} \to \partial K$ is its inverse. Let $g : S^{n-1} \cap H \to H$ be the curve defined by $g(v) = \Pi(\gamma(v))$, thus $dg|_u = \langle d\gamma|_u(w), w\rangle$ [7, p. 277].

Now, consider a strictly convex region $\phi \subset \mathbb{R}^n$ with a twice-differentiable boundary such that $\phi \subset K$, and let $f : S^{n-1} \to \partial\phi$ be a differentiable map that assigns to each unit tangent vector $u \in S^{n-1}$ the unique point p in the boundary of ϕ such that u is the unit tangent vector of $\partial\phi$ at p. The curvature $\kappa_\phi(p)$ of $\partial\phi$ at p is given by $\kappa_\phi(p) = \frac{1}{|df|_u|} \in \mathbb{R}$, where $|df|_u|$ is the determinant of the inverse Weingarten map (see Definition 1.1.17).

We aim to prove that if the curvature at a point p on the boundary of the convex body K is *strictly* positive, i.e., $\kappa_K(p) > 0$, then its $(n-1)$-projection has a strictly positive Gauss curvature at $\pi_{u^\perp}(p)$. Since the Gaussian curvature is the product of principal curvatures, it suffices to show that the projection of K, $g(p)$, into the hyperplane H generated by the vectors $u, w \in \mathbb{S}^{n-1}$ has a strictly positive curvature for any tangent vector w of K at p.

Let $\kappa_K(p)$ be the curvature of K at p, and $\kappa_\Pi(g(p))$ be the curvature of the projection of p onto H. Since $dg|_u = \langle d\gamma|_u(w), w\rangle$, and $\kappa_\phi(p) = \frac{1}{|d\gamma|_u}$, we have $\kappa_K(p) = \langle d\gamma|_u(w), w\rangle$.

Now, we know that $\kappa_\Pi(g(p)) = \frac{1}{|dg|_u|}$, and since w is a unit tangent vector, then $\langle w, w\rangle = 1$. Substituting in the expression for $dg|_u$, we obtain that $\frac{1}{\langle d\gamma|_u(w),w\rangle} = \frac{1}{|d\gamma|_u|\langle w,w\rangle} = \frac{1}{|d\gamma|_u|} = \kappa_\Pi(g(p))$. From the assumption that $\kappa_K(p)$ is *strictly* positive, it follows that this equivalence yields that the curvature of any 2-dimensional projection $\kappa_\Pi(g(p))$ must also be *strictly* positive, implying that all principal curvatures of the $(n-1)$-projection of K are positive. In fact, note that it

is enough to have one positive principal curvature of the $(n-1)$-projection to rule out that the $(n-1)$-projection of K is a simplex.

Hence, the $(n-1)-$dimensional projection of K in a plane containing the tangent vector w also contains this $2-$ dimensional projection. Hence, the projected body in $(n-1)-$ dimension contains at least one direction of positive principal curvature. Considering that simplices in $\mathbb{R}^{n-1}$ are polytopes, their boundary has null curvature. This means that principal curvatures are zero on planar regions. Thus, if there exists a point $p \in \text{proj}_{u^\perp}(K)$ for some $u \in \mathbb{S}^{n-1}$ for which the Gauss curvature exists and is strictly positive, then $\text{proj}_{u^\perp}(p)$ cannot belong to a simplex.

After showing that for any convex body $K \subset \mathbb{R}^n, n \geq 3$, there exists a vector $u \in \mathbb{R}^{n-1}$ such that

$$\frac{V_{n-1}(\text{proj}_{u^\perp}(K) - \text{proj}_{u^\perp}(K))}{V_{n-1}(\text{proj}_{u^\perp}(K))} < \binom{2(n-1)}{n-1}. \tag{2.3}$$

The aim is to now extend this single direction u to an open set of vectors on $\mathbb{S}^{n-1}$. Using the continuity of the surface area function $V_{n-1}(\cdot)$ with respect to the Hausdorff distance on convex bodies, combined with the continuity and linearity properties of the projection operator $\text{proj}_{u^\perp}(\cdot) : \mathbb{R}^n \to \mathbb{R}^{n-1}$, the composition $V_{n-1} \circ \text{proj}_{u^\perp}(K)$, as a composition of continuous operators, is also continuous for any convex body $K \in \mathbb{R}^n$. Consequently, $\forall \epsilon > 0$, there exists an open set $U \subset \mathbb{S}^{n-1}$ such that:

$$\binom{2(n-1)}{n-1} - \frac{V_{n-1}(\text{proj}_{v^\perp}(K) - \text{proj}_{v^\perp}(K))}{V_{n-1}(\text{proj}_{v^\perp}(K))} > 0$$

holds for all $v \in U$ whenever $\|u - v\|_{\mathbb{S}^{n-1}} < \epsilon$. This, in turn, implies the existence of an open set $U' \subset \mathbb{R}^{n-1}$ such that for every $u \in U'$, $\text{proj}_{u^\perp}(K)$ is not a simplex. Hence, this proves there exists an open set $U \subset \mathbb{S}^{n-1}$ such that $\forall u \in U$, $\text{proj}u^\perp(K) \neq simplex$, which yields strict inequality in (2.2).

Thus, in both cases, whether K is a polytope with $n+1$ vertices or K contains a non planar region, there exists an open set $U \in \mathbb{S}^{n-1}$ such that, $\forall u \in U$,

$$V_{n-1}(\mathrm{proj}_{u^\perp}(K) - \mathrm{proj}_{u^\perp}(K)) < \binom{2(n-1)}{(n-1)} V_{n-1}(\mathrm{proj}_{u^\perp}(K)),$$

which in turn implies that, for $n \geq 3$,

$$S(K-K) < \binom{2(n-1)}{(n-1)} S(K).$$

Chapter 3

Further upper bound estimates in $\mathbb{R}^3$

In this section, we calculate the surface area of a parameterized family of convex bodies in $\mathbb{R}^3$ in an attempt to gain more insight into the bounds of the surface area of difference bodies in relation to the upper bound determined in (2.2). Since the bound obtained is not reached, we want to study if the bound is asymptotically reached and for what shape that may occur.

In the first part, we analyse the behaviour of the difference body $K - K$ as K continuously transitions from a cube to a simplex, thus from a centrally symmetric polyhedron to one that is known to be the most *asymmetric* polyhedron, in fact the most asymmetric convex body in $\mathbb{R}^3$ as several classical measures of symmetry characterize it [11, p. 138].

In the second section, we calculate the surface area ratios of $K - K$ to K for certain bodies in $\mathbb{R}^3$ where this is relatively simple to do. Finally, using various codes in Python, we calculate the surface area of the difference body in $\mathbb{R}^3$ for different types of polyhedra. Using this, we verify that when $n = 3$, the upper bound in (2.2) indeed holds.

For simplicity, given the variation of the upper bound constant obtained for these different bodies, we will refer to the bound as C_K, i.e.

$$C_K := \frac{S(K-K)}{S(K)}. \tag{3.1}$$

3.1 Cube with a corner cut off

The exploration of difference bodies' volume, as denoted by equations (1.2) and (1.3), has provided valuable insights. It is established that the lower bound for the volume occurs when the set K is centrally symmetric, while the upper bound is observed when K is a simplex. As part of an undergraduate honors project [8], we delved into the behavior of the volume of $K-K$ as K transitions from a cube to a simplex. This transition also has implications for the ratio of surface areas. The analysis sheds light on how these geometric transformations influence the relationship between the volumes and surface areas of the original and difference bodies.

The transition was performed by cutting a corner off a cube of side 2 with a plane of normal direction $\langle 1,1,1\rangle$, and when that corner's dimensions are exhausted, we start cutting along the edges orthogonal to the edges previously exhausted. Finally, exhausting these subsequent edges yields the right tetrahedron.

We define and study a continuous function $C_{K_\mu}(\mu) = \frac{S(K_\mu - K_\mu)}{S(K_\mu)}$ as we consider the convex body K_μ, $0 \le \mu \le 4$, and how it affects the difference body $K_\mu - K_\mu$. We start with a cube C of side length 2 in $\mathbb{R}^3$, defined as the following convex hull:

$$C = \text{conv}\{(0,0,0),(0,2,2),(0,2,0),(0,0,2),(2,2,0),(2,2,2),(2,0,2),(2,0,0)\}.$$

We now define the body K_μ. For $\mu = 0$, we have the originally defined cube, and as μ increases, we lose symmetry as we cut along the three edges intersecting at

$(0, 2, 2)$. This cutoff portion is the tetrahedron with vertices $(0, 2-\mu, 2)$, $(0, 2, 2-\mu)$, and $(\mu, 2, 2)$, $0 \leq \mu \leq 2$.

When we reach $\mu = 2$, we exhaust the edges along which we previously cut as can be observed in Figure 3.1.2, and we start cutting along the edges orthogonal to the exhausted edges. When we reach $\mu = 4$, K_μ is finally a simplex, in this case a trirectangular tetrahedron.

Due to the change in K_μ's shape when we exhaust the initial three edges, we obtain two different sets of equations for the surface areas $S(K)$ and $S(K-K)$:

$$S(K_\mu) = \begin{cases} 8 + \frac{\mu^2}{2}(\frac{\sqrt{3}}{3} - 1) & 0 \leq \mu \leq 2 \\ \frac{\sqrt{3}}{3}(2 + 2(\mu-2) - (\mu-2)^2) - 2(\mu-2) + 6 & 2 \leq \mu \leq 4 \end{cases}$$

and

$$S(K_\mu - K_\mu) = \begin{cases} 32 + \mu^2(\frac{\sqrt{3}}{3} - 1) & 0 \leq \mu \leq 2 \\ \frac{1}{3}(-2\sqrt{3}(\mu-2)^2 + (\mu-2)(4\sqrt{3} + 12\sqrt{2} - 36) + 4\sqrt{3} + 84) & 2 \leq \mu \leq 4 \end{cases}.$$

Using these equations yields the following constant C_{K_μ}:

$$C_{K_\mu} = \begin{cases} \dfrac{32 + \mu^2(\frac{\sqrt{3}}{3} - 1)}{8 + \frac{\mu^2}{2}(\frac{\sqrt{3}}{3} - 1)} & 0 \leq \mu \leq 2 \\ \dfrac{\frac{1}{3}(-2\sqrt{3}(\mu-2)^2 + (\mu-2)(4\sqrt{3} + 12\sqrt{2} - 36) + 4\sqrt{3} + 84)}{\frac{\sqrt{3}}{3}(2 + 2(\mu-2) - (\mu-2)^2) - 2(\mu-2) + 6} & 2 \leq \mu \leq 4. \end{cases}$$

Using these equations, we can now observe C_{K_μ}'s behaviour through the graph displayed in Figure 3.1.1.

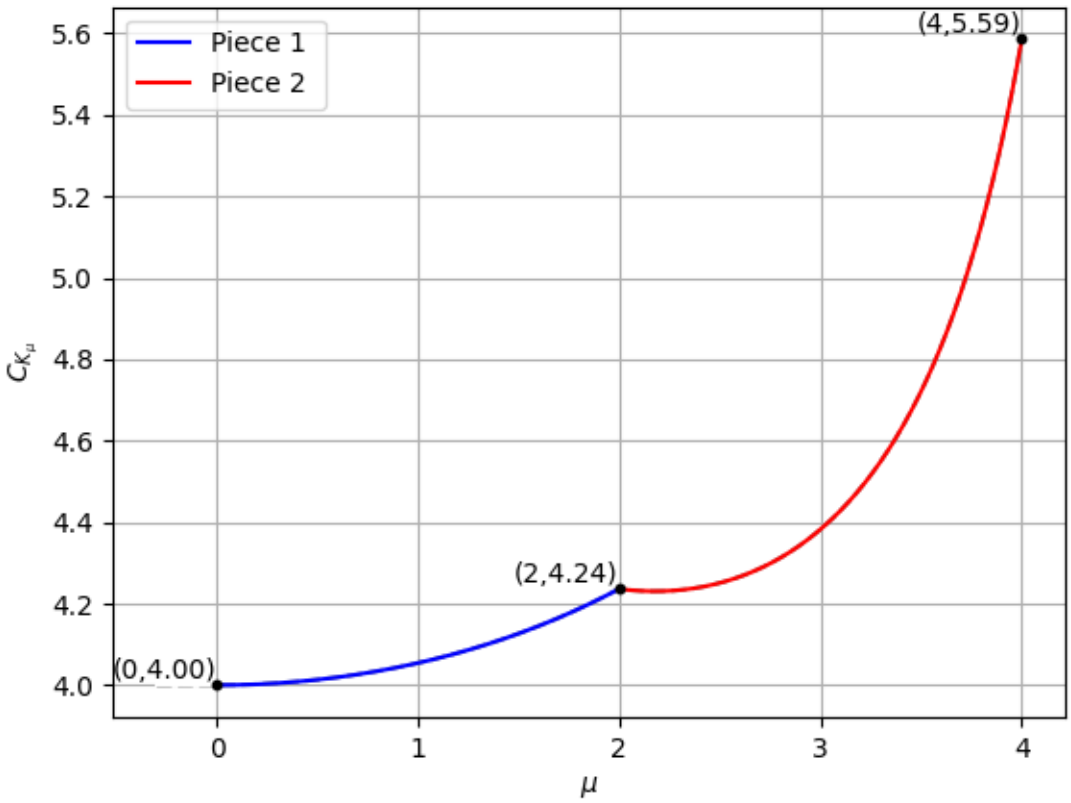

Figure 3.1.1: C_{K_μ}

We observe that as we remove portions from K_μ, the constant C_{K_μ} consistently increases. Notably, the following points are highlighted:

- As expected, when K_0 is a cube, the central symmetry contributes to achieving the smallest constant. This illustrates the impact of central symmetry on the lower bound for C_{K_μ}.

- The constant C_{K_μ} experiences a moderate increase for $0 \leq \mu \leq 2$, indicating that K_μ remains somewhat symmetric during this interval. Interestingly, there is a local maximum at $\mu = 2$. From Figure 3.1.2, we see that one of K's facets (the facet orthogonal to the normal $\langle 1, 1, 1 \rangle$) is an equilateral triangle. Beyond $\mu = 2$, when we start cutting further, the facet is no longer a triangle,

as three new edges are formed. This suggests that K_μ gains a slight temporary enhancement in symmetry from the loss of the simplical face within a small interval $\mu \in (2, 2+\epsilon), \epsilon > 0$, explaining C_{K_μ}'s local maximum at $\mu = 2$ observed in the graph.

- Beyond this, the increase in C_{K_μ} becomes more exponential as K_μ approaches the shape of a simplex. This upward trend reaches its peak at $\mu = 4$ when K_4 takes the form of a right tetrahedron.

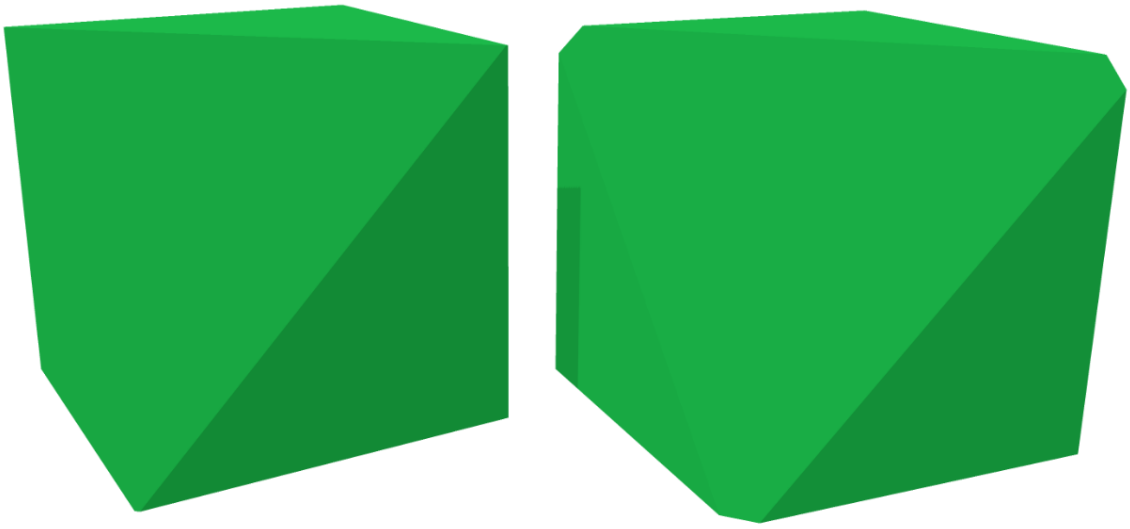

Figure 3.1.2: K_2 on the left, $K_\mu - K_\mu$ on the right for $\mu \in (2, \epsilon), \epsilon > 0$

Hence, observing this continuum of constants C_{K_μ} allows us to observe the continuous effect of symmetry on the surface area of $K - K$, putting an emphasis on the disparity between the cube and the simplex.

3.2 Bodies with fixed constant C_K in $\mathbb{R}^3$

3.3 The cube

Let $C \in \mathbb{R}^3$ be the cube. Since the difference body of a cube is also a cube, the surface area of its difference body is almost immediate. As seen in Section 3.1, we obtained the smallest constant C_{K_μ} for $\mu = 0$ when K_0 is a cube.

It is no coincidence that our lower bound occurs when K_μ is centrally symmetric. Furthermore, the smallest constant $C_{K_0} = 4$, is explained by an interesting property of parallelotopes; the Minkowski sum of three linearly independent line segments is a parallelepiped. When those line segments are orthogonal have equal length, we obtain a cube. If a cube C has side-length c, then its surface area is simply $S(C) = 6c^2$. In other words, let C be the Minkowski sum of three line segments $seg[0, x_1], seg[0, x_2]$, and $seg[0, x_3]$, $\{x_i\}_{i=1}^3 > 0$, assuming without loss of generality that they all start at the origin. Let all three line segments have length c and be pairwise orthogonal. Then:

$$C = seg[0, x_1] + seg[0, x_2] + seg[0, x_3]$$
$$-C = seg[-x_1, 0] + seg[-x_2, 0] + seg[-x_3, 0].$$

Then the Minkowski sum of these cubes yields

$$C - C = seg[-x_1, x_1] + seg[-x_2, x_2] + seg[-x_3, x_3].$$

The Minkowski sum of a line segment with itself yields a line segment twice the length of the original line, hence, $C - C$ is the Minkowski sum of three pairwise orthogonal line segments of length $2c$, which is a cube of side-length $2c$. This yields

$$S(C - C) = S(2C) = 2^2 S(C) = 4(6c^2) = 4S(C).$$

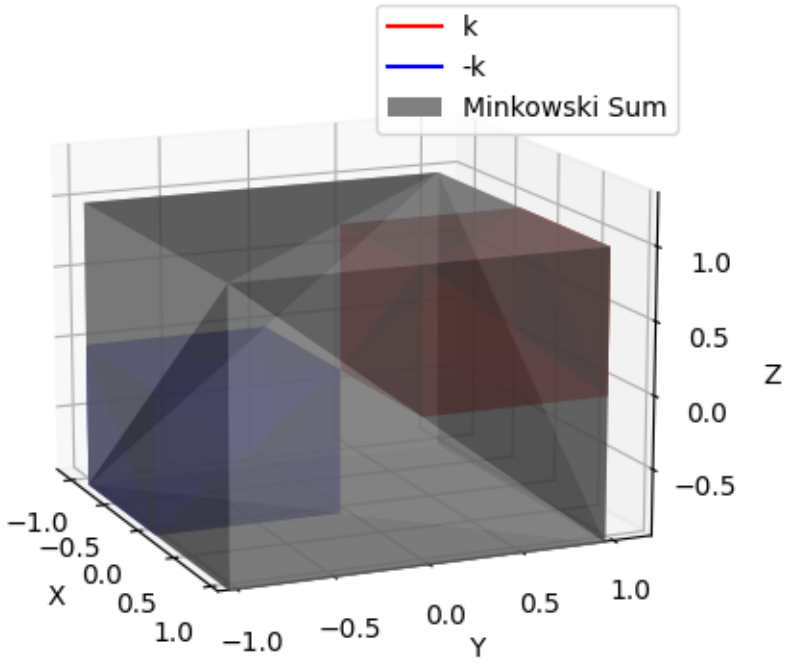

Figure 3.3.1: Difference body of the unit cube

Hence, our constant $C_c = 4.0$.

We see that similarly to the volume ratio of the cube, we get the smallest constant for any K which is a centrally symmetric convex body. This is a very simple consequence of combining the surface area formula with the calculations for the volume of the difference body as explained in Section 2.2. In this case, we know that the cube is centrally symmetric.

3.4 The cylinder

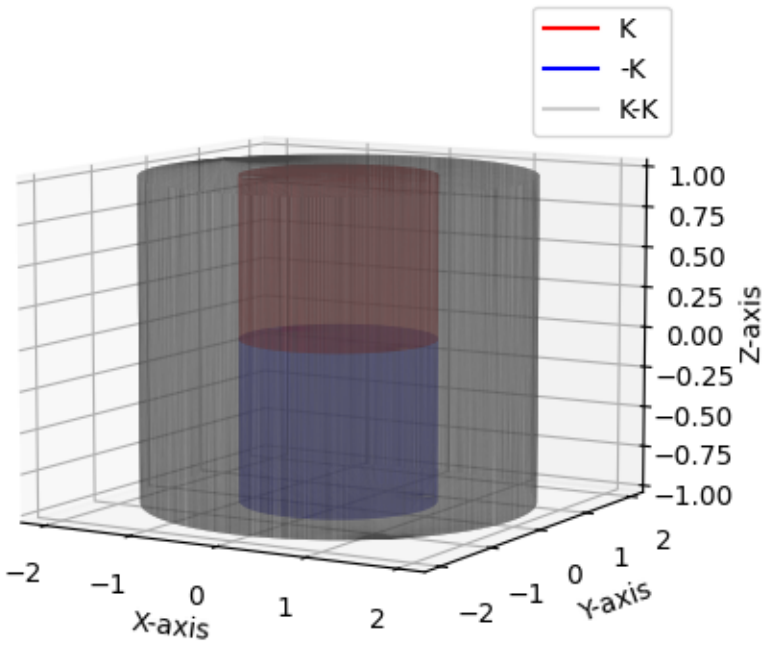

Figure 3.4.1: Difference body for a right cylinder of unit height and unit radius

Let K be the cylinder in $\mathbb{R}^3$ with radius r and height h. By central symmetry of the cylinder, the difference body is simply the Minkowski sum of a cylinder with

itself. Thus, $K - K$ yields another larger cylinder of radius $2r$ and height $2h$. Then by a simple calculation, we obtain the following surface areas:

$$S(K) = 2\pi rh + 2\pi r^2$$
$$S(K - K) = 2\pi(2r)(2h) + 2\pi(2r)^2,$$

and the ratio yields

$$\frac{S(K-K)}{S(K)} = \frac{2\pi(2r)(2h) + 2\pi(2r)^2}{2\pi rh + 2\pi r^2} = 4\frac{2\pi rh + 2\pi r^2}{2\pi rh + 2\pi r^2} = 4.$$

3.5 The regular simplex

Since one of the most researched and simplest convex body to work with is the simplex, it is only logical to start by approximating its upper bound.

Since we are often considering simplices in $\mathbb{R}^n$ for $n \leq 3$, we define the simplex in those dimensions separately: a simplex in $\mathbb{R}$ is a line segment, in $\mathbb{R}^2$, a triangle and, in $\mathbb{R}^3$, a tetrahedron.

Let T be a regular simplex of unitary side length. Without loss of generality, we place one of its vertices at the origin. Then we define T and $-T$ as the convex hull of $n + 1 = 4$ vertices as follows:

$$T = \text{conv}\{(0,0,0), (\tfrac{1}{\sqrt{2}}, 0, \tfrac{1}{\sqrt{2}}), (\tfrac{1}{\sqrt{2}}, \tfrac{1}{\sqrt{2}}, 0), (0, \tfrac{1}{\sqrt{2}}, \tfrac{1}{\sqrt{2}})\}$$

$$-T = \text{conv}\{(0,0,0), (\tfrac{-1}{\sqrt{2}}, 0, \tfrac{-1}{\sqrt{2}}), (\tfrac{-1}{\sqrt{2}}, \tfrac{-1}{\sqrt{2}}, 0), (0, \tfrac{-1}{\sqrt{2}}, \tfrac{-1}{\sqrt{2}})\}.$$

The resulting body obtained from the Minkowski sum $T - T$ can be observed in Figure 3.5.1, and is called a *cuboctahedron*. It is a convex body composed of 12

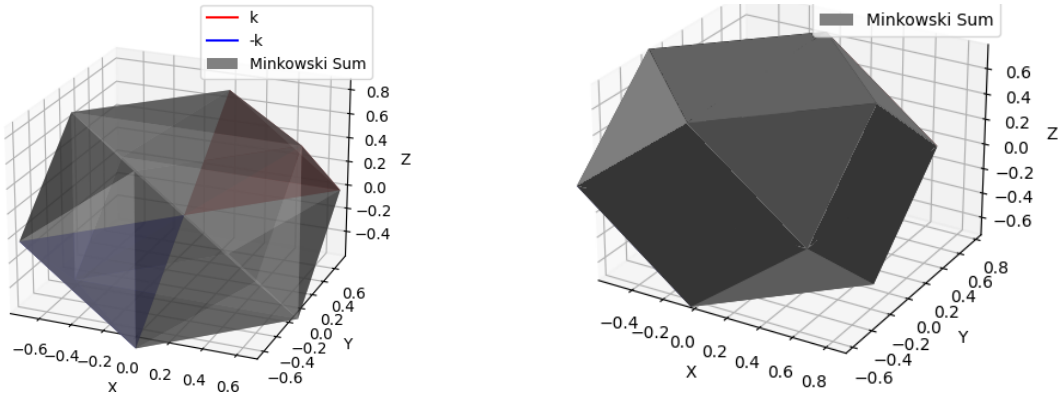

(a) View 1: K and $-K$ inside $K - K$ (b) View 2: $K - K$

Figure 3.5.1: Two different views for $T - T$, for the regular unit simplex T

vertices, 24 edges, and 14 faces. From that pool of faces, 8 are the faces from T and $-T$, while the 6 remaining faces are quadrilateral faces. In our case, through T's regularity, $T - T$'s edges all have unit length. The formation of these quadrilateral faces will be discussed further in Section 3.6.

Note: For reasons concerning optimization, we see from Figure 3.5.1 (view 1) that non-triangular faces are sometimes split into triangles as a consequence of the `ax.plot_trisurf` *command, which describes our figure three vertices at a time. It chooses the closest ones forming a simplex in* $\mathbb{R}^2$ *before computing the convex hull of these figures in* $\mathbb{R}^3$ *using* `scipy.spatial.ConvexHull`.

The convex difference body $T - T$ is separated into two parts of equal volume and surface area, each containing the faces of T, separated by the previously described quadrilateral faces. By embedding T and $-T$ in $T - T$, Figure 3.5.1 allows us to compare the dimensions of the original body and the difference body. The code (see Appendix 3.1) also provides us with T's, $-T$'s, and $T - T$'s vertices. Using the location of these bodies in space, we are able to show that if T's height is h, $T - T$ has height $2h$. We also see that T and $-T$ share the same apex at the origin.

When running the code, we see that the surface area obtained for the dif-

ference body $S(T-T) \approx 9.464101615137753$, while the surface area $S(T) = \sqrt{3}$. This can easily be verified, as $S(T-T) = 2S(T) + 6$. $2S(T)$ corresponds of the surface area of the 8 faces from T and $-T$ that carry over to $T-T$, and the leftover six quadrilateral faces of unit side length give us $6 =$ *surface area of (each of) the quadrilateral faces*. Hence,

$$C_T = \frac{S(T-T)}{S(T)} = \frac{2\sqrt{3}+6}{\sqrt{3}} \approx 5.464101615137755.$$

This holds for any regular tetrahedrons of side length a, since $S(T) = \sqrt{3}a^2$ and $S(T-T) = 2\sqrt{3}a^2 + 6a^2$ yields

$$C_T = \frac{S(T-T)}{S(T)} = \frac{2\sqrt{3}a^2+6a^2}{\sqrt{3}a^2} = \frac{2\sqrt{3}+6}{\sqrt{3}} = 2 + 2\sqrt{3} \approx 5.464101615137755,$$

which leaves much room for improvement with regards to approaching the prescribed upper bound in (2.2). However, unlike the classical Rogers-Shephard inequality which results in a ratio of volumes invariant under linear transformations of $\mathbb{R}^3$ whose determinants have absolute value 1, the ratio of surface areas is not invariant, and so a simplex which is not regular will likely yield a different value constant.

In fact, this illustrates a significant difference between the classical Rogers-Shephard inequality which yields the same constant for K and any of its affine images and the surface area Rogers-Shephard type inequality that we derived in this work for which the constant $C(K)$ is, generally, different from $C(TK)$ for an affine transformation $T : \mathbb{R}^n \to \mathbb{R}^n$.

3.6 Pyramidal bodies

In this section, we start to manipulate the dimensions of K to observe more interesting patterns and results. Since it is more difficult to keep track of any patterns using the previous Python code in which we input specific vertices, we wrote a second

Python code (see Appendix 3.2) that allows us to uniformly distribute m vertices along the boundary of a disk of radius r centered at the origin, with the $(m+1)$'th vertex at $(0, 0, h)$ for some positive height h.

We start with the simplex, which has $m = 3$ vertices in the base. Here, we are interested in non-regular simplices and how they compare to the previous results obtained for a regular simplex T. Next, we proceed with pyramids containing an even number of vertices forming the base, followed by pyramids with an odd number of vertices at the base.

3.7 Triangular pyramid/simplex: $m = 3$

Let

$$m = 3$$

$$r = 1$$

$$h = 1.$$

The resulting body $K - K$ can be observed in Figure 3.7.1 through two different views: the first allowing us to see through $K - K$ to compare its dimensions to that of K, and the second view allows for clear observation of the difference body's facets. The body $K - K$ contains 12 vertices, 24 edges, and 14 faces. We notice that its composition is that of the regular simplex in Section 3.5. We observe that $K-K$'s 14 faces consist of 8 triangular faces coming from K and $-K$, while the remaining facets are quadrilateral. The equilateral bases of the original simplices are on opposite ends of $K - K$, and serve as its bases. From these bases emerge the lateral faces, which are composed of the remaining faces of K and $-K$ *(isosceles triangles)*, separated by

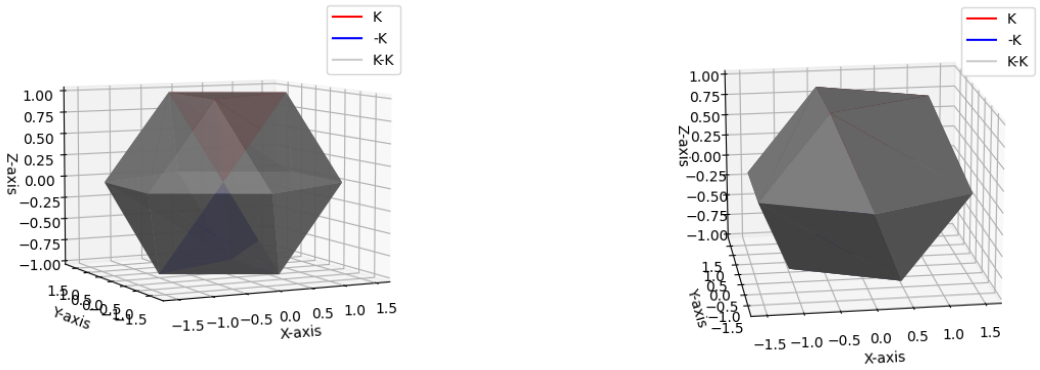

(a) View 1: K and $-K$ inside $K - K$

(b) View 2: $K - K$

Figure 3.7.1: Two different views of $K - K$ for $m = 3$

the 6 remaining quadrilateral faces.

These quadrilateral faces reveal an interesting behaviour of the Minkowski sum of the difference bodies of simplices. If we choose the equilateral face in K to be its base, then these quadrilaterals *(parallelograms)* have length equal to the base length in K, and their height is equal to the lateral edge length in K. This can be observed in Figure 3.7.1 (view 1). We see that the quadrilateral's length and K's base share an edge, while K's lateral edge is shared with the quadrilateral's height.

Finally, with the chosen parameters above, we obtain a constant C_K comparable to the constant obtained for the regular tetrahedron.

Here, $S(K) \approx 4.203775615332221$, and $S(K - K) \approx 23.104489687363515$, which yields a constant $C_K \approx 5.496128195590569$. There is no significant discrepancy between this constant and the constant obtained for the regular simplex ($C_T \approx 5.464101615137755$). We also have much room for a potentially greater constant that would allow us to approach the projected upper bound. Since we were able to obtain a better estimate for this simplex after computing C_T for the regular tetrahedron, this suggests that there exist convex bodies which would allow us to obtain better constants.

We now generalize this result for varying radii r and heights h:

Table 3.7.1: Numerical results for $m = 3$

K_i	R	h	$S(K_i)$	$S(K_i - K_i)$	C_{K_i}
K_0	1	1	4.204	23.104	5.496
K_1	5	1	67.454	399.860	5.928
K_2	50	1	6497.788	38981.533	5.9992
K_3	500	1	649521.651	3897124.709	5.999992
K_4	10000	1	259807623.733	1558845737.204	5.99999998
K_5	1	5	14.354	81.699	5.692
K_6	1	50	131.209	782.138	5.961
K_7	1	500	1300.338	7796.838	5.996
K_8	1	10000	25982.061	155887.171	5.9998

Observing the values in Table 3.7.1, we note that C_{K_i} is steadily increasing as R increases when $h = 1$. The same pattern is observed when $R = 1$ and h is steadily increasing. We must also note that C_{K_i} is also quite large for all $i \in \{0, \ldots, 8\}$. Similarly to the case of the Rogers-Shephard inequality (1.3), this can be explained by the asymmetry of the simplex in the class of convex bodies.

Let T be K's base, the equilateral triangle. Geometrically, as $R \to \infty$, K collapses onto the base T, and a second triangular base is created on top of the original one from the originally lateral faces. The radius grows larger, and if T has side length s, $S(K)$ can then be written as $S(K) = 2S(T) = 2(\frac{\sqrt{3}}{4}s^2)$. Per the Rogers-Shephard inequality (1.3), we know that in $\mathbb{R}^2$, $V_3(T - T) = 6V_3(T)$ for any triangle T. Since each of the now superposed bases is an equilateral triangle, then $\lim_{R\to\infty} C_K$ can be easily computed:

$$\lim_{R\to\infty} C_K = \lim_{R\to\infty} \frac{S(K-K)}{S(K)} = \frac{6(2A(B))}{2A(B)} = 6.$$

We will see in the following sections how veering away from asymmetry by manipulating the number of vertices around K's base substantially affects the range of C_{K_i}.

3.8 Evenly distributed vertices around a circular base: m_{even}

For this part, we calculate C_K, C_L, C_A, and C_B for four different bodies for which we test a varying even number of vertices around the base, and vary the values for R and h. We first present the numerical results in four tables, followed by the geometric analysis of the obtained difference bodies.

Table 3.8.1: Numerical results for $m = 4$

K_i	R	h	$S(K_i)$	$S(K_i - K_i)$	C_{K_i}
K_0	1	1	5.464	24.785	4.536
K_1	5	1	101.962	411.769	4.038
K_2	50	1	10001.999	40011.998	4.0004
K_3	500	1	1000002	4000012	4.000004
K_4	10000	1	400000002.0	1600000012.0	4.00000001
K_5	1	5	16.283	89.697	5.509
K_6	1	50	143.435	852.613	5.944
K_7	1	500	1416.215	8489.289	5.994
K_8	1	10000	28286.271	169709.628	5.9997

Table 3.8.2: Numerical results for $m = 6$

L_i	R	h	$S(L_i)$	$S(L_i - L_i)$	C_{L_i}
L_0	1	1	6.567	29.008	4.417
L_1	5	1	131.61	529.873	4.026
L_2	50	1	12992.113	51971.915	4.00027
L_3	500	1	1299039.838	5196162.815	4.0000027
L_4	10000	1	519615244.003	2078460979.475	4.000000007
L_5	1	5	17.821	96.536	5.417
L_6	1	50	152.621	905.331	5.932
L_7	1	500	1502.600	9005.210	5.993
L_8	1	10000	30002.598	180005.197	5.9997

Table 3.8.3: Numerical results for $m = 10$

A_i	R	h	$S(A_i)$	$S(A_i - A_i)$	C_{A_i}
A_0	1	1	7.203	31.465	4.368
A_1	5	1	148.553	597.427	4.022
A_2	50	1	14696.256	58788.272	4.00022
A_3	500	1	1469464.755	5877862.271	4.0000022
A_4	10000	1	587785253.917	2351141018.917	4.000000006
A_5	1	5	18.667	100.245	5.370
A_6	1	50	157.475	933.097	5.925
A_7	1	500	1548.027	9276.404	5.992
A_8	1	10000	30904.639	185416.075	5.9996

Table 3.8.4: Numerical results for $m = 100$

B_i	R	h	$S(B_i)$	$S(B_i - B_i)$	C_{B_i}
B_0	1	1	7.581	32.925	4.343
B_1	5	1	158.532	637.241	4.020
B_2	50	1	15699.201	62799.946	4.00020
B_3	500	1	1569764.560	6279061.381	4.000002
B_4	10000	1	627905196.864	2511620790.600	4.000000005
B_5	1	5	19.156	102.376	5.344
B_6	1	50	160.225	948.790	5.922
B_7	1	500	1573.681	9429.526	5.992
B_8	1	10000	31413.899	188470.834	5.9996

First, we notice that for all chosen even m values, our constants behaves similarly: when $h = 1$, as R increases, C_{K_i}, C_{L_i}, C_{A_i}, and C_{B_i} are all decreasing, reaching the smallest constant for $i = 4$. For the four bodies, the pattern shows that we are approaching the limiting value 4.0.

Next, when $R = 1$ is constant, and we increase h, we see that our constants C_{K_i}, C_{L_i}, C_{A_i}, and C_{B_i} are all increasing. When $i = 8$, we obtain our largest constants across all four bodies, which are approaching the desired upper bound $C_K = 6$.

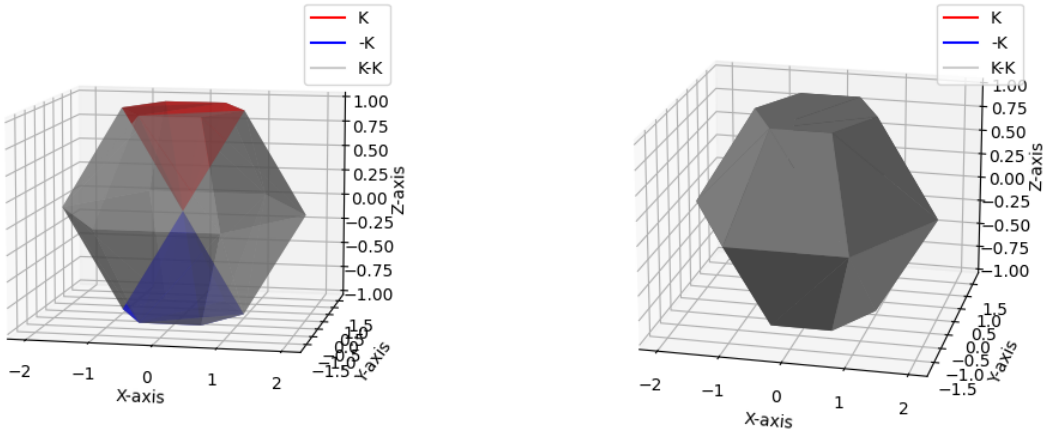

(a) View 1: L_0 and $-L_0$ inside $L_0 - L_0$

(b) View 2: $L_0 - L_0$

Figure 3.8.1: Two different views of $L_0 - L_0$ for $m = 6$

Note: For visualization purposes, we chose $m = 6$ to allow the reader to follow our observations before generalizing them to m_{even}.

In this first round of observations, we chose $m = 6, h = 1, R = 1$ for our analysis, which corresponds to the body L_0, a hexagonal pyramid. From Figure 3.8.1 we see that $L_0 - L_0$ has the shape of two frustums of a pyramid with 6 lateral faces attached at the lower base. This base M, which is also L_0's base, has side length s and apothem length r, which is also its inradius. Hence, $S(M) = \frac{6sr}{2}$

From the frustum's upper base M emerge 6 lateral faces. These lateral faces are the isosceles trapezoids T. If L_0 has slant height l and base edge length s, then T has height l, bottom base length $2s$, and top base length s. Hence,

$$S(T) = \frac{3sl}{2}.$$

As for L_0, since it has slant height l and base edge length s, then

$$S(L_0) = \frac{6sr+6sl}{2} = \frac{6s(r+l)}{2}.$$

Compiling all this information, each frustum has surface area $S(M)+6S(T)$, which allows us to obtain the formula for the surface area of $L_0 - L_0$ when $m = 6$:

$$S(L_0) = \frac{6s(r+l)}{2}$$

$$S(L_0 - L_0) = 2S(M) + 26S(T) = 6sr + 18sl.$$

We also know that $h = 1$ and $R = 1$. Using basic trigonometric identities, we get that $r = \frac{\sqrt{3}}{2}$, $l = \frac{\sqrt{7}}{2}$ and $s = 1$. Hence,

$$\begin{aligned} C_{L_0} = \frac{S(L_0 - L_0)}{S(L_0)} &= \frac{6sr + 18sl}{\frac{6s(r+l)}{2}} \\ &= \frac{6\frac{\sqrt{3}}{2} + 18}{(1 + \frac{\sqrt{7}}{2})} \\ &= \frac{2\frac{\sqrt{3}}{2} + 6\frac{\sqrt{7}}{2}}{\frac{\sqrt{3}}{2} + \frac{\sqrt{7}}{2}} \\ &= \frac{2\sqrt{3} + 6\sqrt{7}}{\sqrt{3} + \sqrt{7}} \\ &\approx 4.417 \end{aligned}$$

which confirms the result indicated in the table obtained with the code.

Now, we want to generalize this result for any pyramid K with an even number of vertices around the base. Since m_{even} is even, by convention, we let K have $2k$ vertices around the base, $k \in \{2, 3, \dots\}$, which yields:

$$S(K) = \frac{2ks(r+l)}{2}$$

$$S(K-K) = 2ksr + 6ksl$$

hence,

$$\begin{aligned} C_K = \frac{S(K-K)}{S(K)} &= \frac{2ksr + 6ksl}{\frac{2ks(r+l)}{2}} \\ &= \frac{ks(2r+6l)}{ks(r+l)} \\ &= \frac{2r+6l}{r+l}. \end{aligned}$$

We then obtain the desired constant $C_K = \frac{2r+6l}{r+l}$, and we can observe that it does not depend on the number of vertices around the base, or on the base length s. This constant is only dependent on the slant height l, and the inradius r.

We are now interested in the asymptotic behaviour of C_K when the limit is taken with respect to the variables in C_K. In this case, C_K is dependent on r and on l. We first make note of the fact that if the limit is taken with respect to r, l also goes to infinity. For this reason, we need to use a change of variable to take appropriate limits.

The relation $l^2 = h^2 + r^2$ allows us to let $r = l\cos\theta$, which yields $l = \frac{r}{\cos\theta}$. We obtain the following modified equation:

$$C_K = \frac{S(K-K)}{S(K)} = \frac{2r+6l}{r+l} = \frac{2r+6\frac{r}{\cos\theta}}{r+\frac{r}{\cos\theta}} = \frac{2\cos\theta+6}{\cos\theta+1} = 2 + \frac{4}{\cos\theta+1}.$$

Now, C_K depends only on the variable θ. We then need to consider how the angle θ between the slant height l and the inradius r behaves. First, we need to establish bounds for θ. Per the geometry of pyramids, we have that $0 < \theta < \frac{\pi}{2}$. Obviously, from the relationship $l = \frac{r}{\cos\theta}$, if $\theta \to \frac{\pi}{2}$, $l \to \infty$. In that case, h also approaches infinity, h and l become parallel, and K is unbounded. Furthermore, if $\theta \to 0$, then $r = l$. In this case, the base becomes an unbounded regular polygon, and the equality is only possible if the slant height forms the radius of a second base superposed on K's base. In either case, K is no longer a compact body. Clearly, when considering the limit as $r \to \infty$, then $l \to \infty$ as well, and since the height h remains unchanged, θ approaches zero. Hence, we can evaluate the respective limits with the appropriate corresponding angle θ. First, we deal with the inradius r:

$$\lim_{r\to\infty} \frac{S(K-K)}{S(K)} = \lim_{r\to\infty} \frac{2r+6l}{r+l} = \frac{2\cos\theta+6}{\cos\theta+1}_{|\theta=0} = 2 + \frac{4}{\cos\theta+1}_{|\theta=0} = 2 + \frac{4}{1+1} = 4.$$

Initially, as $r \to \infty$, K's base is tending towards an infinite regular m_{even}-gon. This affects the slant length l, as it is now also tending to infinity. It becomes parallel to the base, and a second base is formed on top of the initial one, with $r = l$. Then the surface area of K is the surface area of two superposed regular polygons, i.e., $S(K) = 2\frac{msr}{2} = msr$. Then the Minkowski sum of a regular m_{even}-gon, with its mirrored image yields the same m_{even}-gon with inradius $2r$ and side length $2s$, which has surface area $\frac{m(2r)(2s)}{2}$, and once again, which needs to be considered twice for $S(K-K)$. Hence, we can rewrite the limit as follows:

$$\lim_{r\to\infty} \frac{S(K-K)}{S(K)} = \lim_{r\to\infty} \frac{2r+6l}{r+l} = \frac{\frac{2m(2r)(2s)}{2}}{\frac{2msr}{2}} = 4,$$

which yields the lower bound obtained when the limit was taken with respect to r.

Note that, for large m, K's base becomes circular, and K tends towards a cone. This is explored later on in Section 3.10.

Now, it remains to apply the limit with respect to l:

$$\lim_{l\to\infty} \frac{S(K-K)}{S(K)} = \lim_{l\to\infty} \frac{2r+6l}{r+l} = \frac{2l\cos\theta + 6l}{l\cos\theta + l}_{|\theta=\frac{\pi}{2}} = 2 + \frac{4}{\cos\theta + 1}_{|\theta=\frac{\pi}{2}} = 2 + \frac{4}{1} = 6.$$

For the upper bound, we are able to obtain a limiting constant $C_K = 6$ when θ approaches $\frac{\pi}{2}$. Evidently, that only occurs when K's lateral faces form an angle $\theta = \frac{\pi}{2}$ with the base. In such a case, we lose K's apex, as that particular vertex tends to infinity due to h being dependent on l. If $l \to \infty$, then $h \to \infty$ as well. If both tend to infinity, not only is K unbounded, $K - K$ is also unbounded. Indeed, as $l \to \infty$, $K - K$ will progressively tend to a regular base with m vertices connecting two infinite cones extending in opposite directions along the z-axis. Obtaining an angle $\theta = \frac{\pi}{2}$ implies that K degenerates into an infinite conic right prism with a regular base with m_{even} vertices.

Now, since our code is dependent on the height h and the circumradius R of the pyramid, it would be preferable to apply a change of variable to obtain equations dependent on the variables R and h for comparison purposes. To do so, we can use elementary trigonometric identities.

We know that the inradius r and the height h form a right triangle with hypotenuse l, and by a simple application of the Pythagorean Theorem, $l = \sqrt{h^2 + r^2}$. As for r, considering that it forms a right triangle with R and s, R acting as the hypotenuse and r as the opposite side, changing it would involve adding the variable s to our ratio. Hence, taking the limit $R \to \infty$ implies taking the limit $s \to \infty$. Knowing that $R^2 = r^2 + (\frac{s}{2})^2$, we can use the angle δ between R and s to obtain the relationship $\sin\delta = \frac{r}{R}$. Putting all of these modifications together, we get

$$
\begin{aligned}
C_K = \frac{S(K-K)}{S(K)} &= \frac{2r+6l}{r+l} \\
&= \frac{2r+6\sqrt{h^2+r^2}}{r+\sqrt{h^2+r^2}} \\
&= \frac{2R\sin\delta+6\sqrt{h^2+R^2\sin^2\delta}}{R\sin\delta+\sqrt{h^2+R^2\sin^2\delta}} \\
&= 2+4\frac{\sqrt{h^2+R^2\sin^2\delta}}{R\sin\delta+\sqrt{h^2+R^2\sin^2\delta}}.
\end{aligned}
$$

With this change of variable, h and R are now independent from each other, and we can take their respective limits separately. Since $\sin\delta$ is bounded, we need not to consider it when taking limits. Hence,

$$
\begin{aligned}
\lim_{h\to\infty}\frac{S(K-K)}{S(K)} &= \lim_{h\to\infty}\left[2+4\frac{\sqrt{h^2+R^2\sin^2\delta}}{R\sin\delta+\sqrt{h^2+R^2\sin^2\delta}}\right] = 2+4=6 \\
\lim_{R\to\infty}\frac{S(K-K)}{S(K)} &= \lim_{R\to\infty}\left[2+4\frac{\sqrt{h^2+R^2\sin^2\delta}}{R\sin\delta+\sqrt{h^2+R^2\sin^2\delta}}\right] = 2+4\frac{\sin\delta}{2\sin\delta}=4.
\end{aligned}
$$

These limits agree with the lower and upper bounds calculated earlier with respect to θ, and agree with the code. Hence, for a convex pyramid with a regular base formed by an even number of vertices, we obtain that

$$
4 < C_K = \frac{S(K-K)}{S(K)} < 6.
$$

The lower bound is obtained when K collapses into its base and forms a second

base superposed on the first one as the outradius $R \to \infty$, and the upper bound can only be obtained for unbounded K.

3.9 Evenly distributed vertices around a circular base: m_{odd}

After dealing with a pyramid K with an even number of vertices m around the base, we test for C_K, C_L, C_A, and C_B for four different bodies for which we keep m an odd constant, and vary R and h.

Table 3.9.1: Numerical results for $m = 5$

K_i	R	h	$S(K_i)$	$S(K_i - K_i)$	C_{K_i}
K_0	1	1	6.158	28.941	4.700
K_1	5	1	120.671	541.056	4.484
K_2	50	1	11890.023	53175.185	4.472
K_3	500	1	1188822.462	5316577.063	4.472137
K_4	10000	1	475528259.964	2126627030.391	4.472136
K_5	1	5	17.263	94.469	5.472
K_6	1	50	149.343	886.589	5.937
K_7	1	500	1471.843	8821.550	5.994
K_8	1	10000	29391.640	176340.332	5.9997

Table 3.9.2: Numerical results for $m = 7$

L_i	R	h	$S(L_i)$	$S(L_i - L_i)$	C_{L_i}
L_0	1	1	6.824	30.830	4.518
L_1	5	1	138.486	586.705	4.237
L_2	50	1	13683.736	57745.408	4.220
L_3	500	1	1368206.780	5773605.808	4.219834
L_4	10000	1	547282039.413	2309438554.43	4.219833
L_5	1	5	18.167	98.281	5.41
L_6	1	50	154.620	916.799	5.929
L_7	1	500	1521.332	9117.048	5.993
L_8	1	10000	30374.598	182236.644	5.9996

Table 3.9.3: Numerical results for $m = 15$

A_i	R	h	$S(A_i)$	$S(A_i - A_i)$	C_{A_i}
A_0	1	1	7.413	32.468	4.380
A_1	5	1	154.104	626.252	4.064
A_2	50	1	15254.218	61701.427	4.0449
A_3	500	1	1525264.006	6169209.611	4.0447
A_4	10000	1	610104966.208	2467680083.560	4.045
A_5	1	5	18.939	101.488	5.359
A_6	1	50	159.014	941.888	5.923
A_7	1	500	1562.391	9362.146	5.992
A_8	1	10000	31189.804	187126.624	5.9996

Table 3.9.4: Numerical results for $m = 105$

B_i	R	h	$S(B_i)$	$S(B_i - B_i)$	C_{B_i}
B_0	1	1	7.581	32.931	4.344
B_1	5	1	158.542	637.417	4.020
B_2	50	1	15700.162	62817.844	4.001
B_3	500	1	1569860.612	6280851.455	4.0009
B_4	10000	1	627943617.994	2512336821.385	4.0009
B_5	1	5	19.156	102.379	5.344
B_6	1	50	160.227	948.805	5.922
B_7	1	500	1573.705	9429.670	5.992
B_8	1	10000	31414.379	188473.717	5.9996

We notice in these tables that the constant C_K for m_{odd} behaves similarly to the constants previously estimated for even m. For $0 \leq i \leq 4$, C_{K_i}, C_{L_i}, C_{A_i}, and C_{B_i} are steadily decreasing towards 4.0, with the smallest constants when $i = 4$. On the other end, when $R = 1$ and we increase h, we see once again that $C_{K_i}, C_{L_i}, C_{A_i}$, and C_{B_i} are all increasing towards 6.0.

In this first round, we consider $m = 5$ for observation purposes and to confirm the results obtained from the code. We choose the body K_0 for which $R = h = 1$. Geometrically, we see in Figure 3.9.1 that $K_0 - K_0$'s composition differs from the even case. Once again, we obtain a body whose upper and lower halves are congruent. Each half has the same base as K_0 with 5 edges from which emerge 5 quadrilaterals constituting the lateral faces of $K_0 - K_0$, separated by 5 triangular faces emerging from each vertex at the base. Upon further observation, we notice that those triangular faces are the lateral faces of K_0 carrying over to $K_0 - K_0$.

The base M has side length s and inradius r, which yields $S(M) = \frac{5sr}{2}$. Using

K's slant height l and the base length s, then $S(K_0) = \frac{5s(r+l)}{2}$.

For a regular pentagon, the side length $s = 2Rsin\frac{\pi}{5} = 2\sin\frac{\pi}{5}$ for $R = 1$, and the in-radius $r = \sqrt{R^2 - (\frac{s}{2})^2} = \sqrt{1 - (\sin\frac{\pi}{5})^2}$. Hence, $S(M) = \frac{5sr}{2} = 5\sin\frac{\pi}{5}\sqrt{1 - (\sin\frac{\pi}{5})^2}$. Lastly, K_0's slant length l is given by $l = \sqrt{h^2 + r^2} = \sqrt{2 - (\sin\frac{\pi}{5})^2}$. Hence,

$$S(K_0) = 5\sin\frac{\pi}{5}\left(\sqrt{1 - \left(\sin\frac{\pi}{5}\right)^2} + \sqrt{2 - \left(\sin\frac{\pi}{5}\right)^2}\right) \approx 6.1579.$$

K_0's lateral faces are isosceles triangle with base s and legs of length c. The rectangular faces in $K_0 - K_0$ have length c and width s. Since we do not have c, we can use the Pythagorean Theorem to find it. Given $c^2 = h^2 + R^2 = 2$, the area of all rectangular faces is simply $5S(R_0) = 5sc = 5s\sqrt{h^2 + R^2}$. Compiling all of this together, we get

$$\begin{aligned}
S(K_0 - K_0) &= 2S(K_0) + 10S(R_0) \\
&= 2S(K_0) + 10s\sqrt{h^2 + R^2} \\
&= 5s(r + l) + 10s\sqrt{h^2 + R^2} \\
&= 10\sin\frac{\pi}{5}\left(\sqrt{1 - \left(\sin\frac{\pi}{5}\right)^2} + \sqrt{2 - \left(\sin\frac{\pi}{5}\right)^2}\right) + 20\sin\frac{\pi}{5}\sqrt{2} \\
&\approx 28.9409.
\end{aligned}$$

Finally,

$$
\begin{aligned}
C_{K_0} &= \frac{S(K_0 - K_0)}{S(K_0)} \\
&= \frac{5s(r+l) + 10s\sqrt{h^2+R^2}}{\frac{5(r+l)}{2}} \\
&= 2 + 4\frac{\sqrt{h^2+R^2}}{r+l} \\
&= 2 + 4\frac{\sqrt{2}}{\sqrt{1-(sin\frac{\pi}{5})^2} + \sqrt{2-(sin\frac{\pi}{5})^2}} \\
&\approx 4.69976,
\end{aligned}
$$

which agrees with the value obtained in Table 3.9.1.

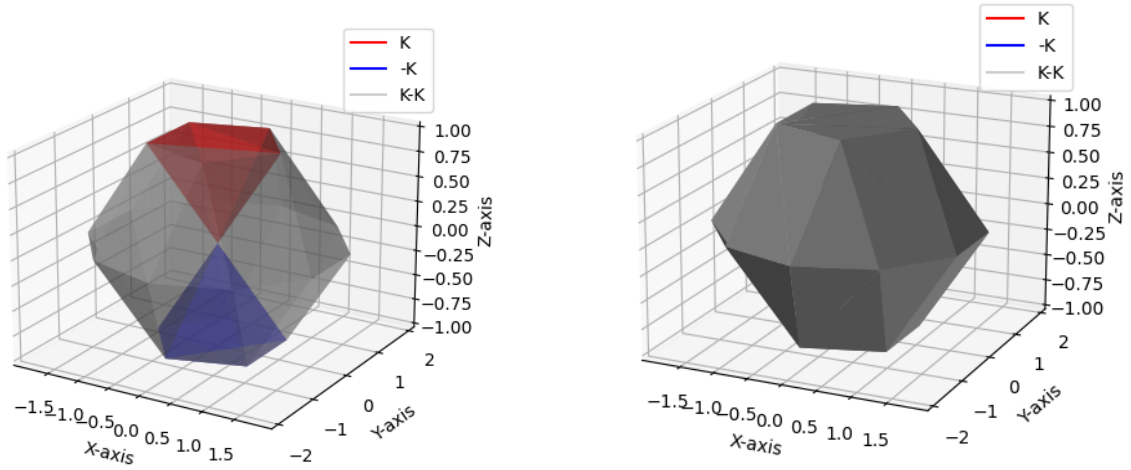

(a) View 1: K_0 and $-K_0$ inside $K_0 - K_0$ (b) View 2: $K_0 - K_0$

Figure 3.9.1: Two different views of $K_0 - K_0$ for $m = 5$

Once again, we want to generalize the result for any pyramid with a regular base comprised of m_{odd} vertices. We know that $S(K-K)$ is comprised of twice the surface area $S(K)$, plus the extra quadrilateral faces that we will denote by Q. Hence, if K has side length s, slant length l, and inradius r, then we have the following formulas for the surface areas of K and $K - K$:

$$
\begin{aligned}
S(K) &= \frac{ms(r+l)}{2} \\
S(K-K) &= 2S(K) + 2mS(Q) \\
&= ms(r+l) + 2ms\sqrt{(\frac{s}{2})^2 + l^2},
\end{aligned}
$$

and since m is odd, we assume that $m = 2k+1, k \in \mathbb{N}, k \geq 1$. Then the corresponding surface areas are

$$
\begin{aligned}
S(K-K) =& 2(2k+1)s\frac{r+l+2\sqrt{(\frac{s}{2})^2+l^2}}{2} \\
S(K) =& \frac{(2k+1)s(r+l)}{2}
\end{aligned}
$$

which yields

$$
\begin{aligned}
C_K = \frac{S(K-K)}{S(K)} =& \frac{2(2k+1)s\frac{r+l+2\sqrt{(\frac{s}{2})^2+l^2}}{2}}{\frac{(2k+1)s(r+l)}{2}} \\
=& 2\frac{r+l+2\sqrt{(\frac{s}{2})^2+l^2}}{r+l} \\
=& 2 + \frac{4\sqrt{(\frac{s}{2})^2+l^2}}{r+l}.
\end{aligned}
$$

We notice that C_K now depends on three variables; r, l, and s.

We can now take the limits with respect to r and l. However, since they are

dependent variables, if we take the limit $r \to \infty$, then we also have $l \to \infty$. Similarly to the previous case, we need to perform a change of variable.

Once again, we have $l = \sqrt{h^2 + r^2}$. Since h and r are independent variables, we should be able to take the limit with respect to each variables when replacing l with this radical expression. Then the corresponding ratio becomes:

$$\begin{aligned} C_K = \frac{S(K-K)}{S(K)} =& 2 + \frac{4\sqrt{(\frac{s}{2})^2 + l^2}}{r + l} \\ =& 2 + \frac{4\sqrt{(\frac{s}{2})^2 + h^2 + r^2}}{r + \sqrt{h^2 + r^2}}. \end{aligned}$$

Since the variable s only appears in the surface area for $K - K$, clearly, taking the limit with respect to s gives us an infinity since only $S(K - K)$ contains s in its formula. But we also know that s depends on r. To deal with it, we consider the relation $(\frac{s}{2})^2 = R^2 - r^2$. Hence

$$\begin{aligned} C_K = \frac{S(K-K)}{S(K)} =& 2 + \frac{4\sqrt{(\frac{s}{2})^2 + h^2 + r^2}}{r + \sqrt{h^2 + r^2}} \\ =& 2 + \frac{4\sqrt{R^2 - r^2 + h^2 + r^2}}{r + \sqrt{h^2 + r^2}} \\ =& 2 + \frac{4\sqrt{R^2 + h^2}}{r + \sqrt{h^2 + r^2}}. \end{aligned}$$

Then, since $\sin\delta = \frac{r}{R}$, the ratio can be changed to

$$C_K = \frac{S(K-K)}{S(K)} = 2 + \frac{4\sqrt{R^2+h^2}}{r+\sqrt{h^2+r^2}}$$
$$= 2 + \frac{4\sqrt{R^2+h^2}}{R\sin\delta + \sqrt{h^2+(R\sin\delta)^2}}.$$

Now, we are able to take successively the limits with respect to R, then with respect to h. However, as $R \to \infty$, r also tends to infinity per their relation by the Pythagorean Theorem. This implies that if both grow to infinity, δ also increases, and is bounded above, reaching a limiting angle of $\frac{\pi}{2}$. But when taking the limit with respect to h, since δ is independent from h, we need not to worry about the limit carrying over to other variables. Now, using the fact that $\sin\delta < 1$, we get

$$\lim_{R\to\infty} \frac{S(K-K)}{S(K)} = \lim_{R\to\infty} \left[2 + \frac{4\sqrt{R^2+h^2}}{R\sin\delta + \sqrt{h^2+(R\sin\delta)^2}} \right]$$
$$= 2 + \frac{4}{\sin\delta(1+\sin\delta)}$$
$$< 2 + \frac{4}{1(1+1)}$$
$$= 4$$
$$\lim_{h\to\infty} \frac{S(K-K)}{S(K)} = \lim_{h\to\infty} \left[2 + \frac{4\sqrt{R^2+h^2}}{R\sin\delta + \sqrt{h^2+(R\sin\delta)^2}} \right]$$
$$= 2 + \frac{4}{1}$$
$$= 6,$$

which yields the same results obtained for m_{even}. Once again, since the code provides the surface area with respect to the height and the radius, by these changes

of variables, we are able to obtain results that strongly correlate with the code. We obtain the same bounds for m_{odd} as we did earlier for m_{even}.

Again, the behaviour for the lower bound as $R \to \infty$ is explained by K's lateral faces forming a second superposed base on top of the original one. These bases are regular polygons with m edges. Hence, the limit can be once again written as follows:

$$\begin{aligned}\lim_{R\to\infty} \frac{S(K-K)}{S(K)} &= \lim_{R\to\infty} \left[2 + \frac{4\sqrt{R^2+h^2}}{R\sin\delta + \sqrt{h^2+(R\sin\delta)^2}}\right] \\ &= \frac{\frac{2m(2r)(2s)}{2}}{\frac{2msr}{2}} \\ &= 4.\end{aligned}$$

As for the upper bound, we once again tend towards it as $h \to \infty$ and we lose K's apex as it becomes an unbounded convex set.

Despite the similarities between the results obtained in the tables, as we increase the radius, we see that the decrease when $h = 1$ is much slower for m_{odd} compared to the values obtained for m_{even}. For example, we see that for $r = 500$, when $m = 6$, $C_{L_3} \approx 4.0000027$, when it is merely $C_{L_3} \approx 4.219834$ when $m = 7$. Furthermore, when increasing r to 10000, C_L decreases dramatically to $C_{L_4} \approx 4.000000007$ for $m = 6$, but stays nearly constant for $m = 7$, going from $C_{L_3} \approx 4.219834$ to $C_{L_3} \approx 4.219833$. Similar behavior can be observed for all bodies, K, L, A, and B for $0 \leq i \leq 4$.

This can be explained by the symmetry in K's base. Indeed, when m is even, K's centrally symmetric base is a regular polygon with m sides. As explained in Section 3.8, as $R \to \infty$, the lateral faces form a second centrally symmetric base

superposed on the original one. When m is odd, the base is not centrally symmetric. Hence, that would explain the slower decrease towards the lower bound, since the lower bound in (2.1) implies that $S(K-K) < 4S(K)$ if K is not centrally symmetric.

Another way to illustrate this difference is by looking at the general formulas for C_K, and comparing the instance when m is even versus odd:

$$C_{K_{even}} = \frac{S(K-K)}{S(K)} = 2 + 4\frac{\sqrt{h^2 + R^2 \sin^2 \delta}}{R \sin \delta + \sqrt{h^2 + R^2 \sin^2 \delta}}$$
$$C_{K_{odd}} = \frac{S(K-K)}{S(K)} = 2 + 4\frac{\sqrt{h^2 + R^2}}{R \sin \delta + \sqrt{h^2 + R^2 \sin^2 \delta}}.$$

The only difference between these constants is the presence of $\sin^2 \delta$ in the radical of the numerator for $C_{K_{even}}$. Through the geometric nature of $K - K$'s formation, we've seen that $0 < \delta < \frac{\pi}{2}$. This angle is between the base edge s and the outradius R. Since $0 < \sin \delta < 1$, then $R^2 \sin^2 \delta < R^2$, and $\sqrt{h^2 + R^2 \sin^2 \delta} < \sqrt{h^2 + R^2}$. The radical in the numerator for $C_{K_{even}}$ is always smaller than that of $C_{K_{odd}}$ if R and h are the same.

3.10 The cone: $m \approx \infty$

Unlike the previous polyhedra, we can easily predict the outcome of the Minkowski sum of the difference body of a cone. Indeed, as we can see in Figure 3.10.1, $K - K$ resembles two frustums of a cone connected at the large base. Each frustum has slant length l, the same as K, and if K's radius is r, then $K - K$ has radius $2r$.

Using the same variables, we obtain the following formulas for the surface areas:

$$S(K) = \pi r^2 + \pi r l$$

$$S(K - K) = 6\pi r l + 2\pi r^2.$$

Then the ratio of the surface areas yields:

$$\frac{S(K-K)}{S(K)} = \frac{6l + 2r}{r + l}.$$

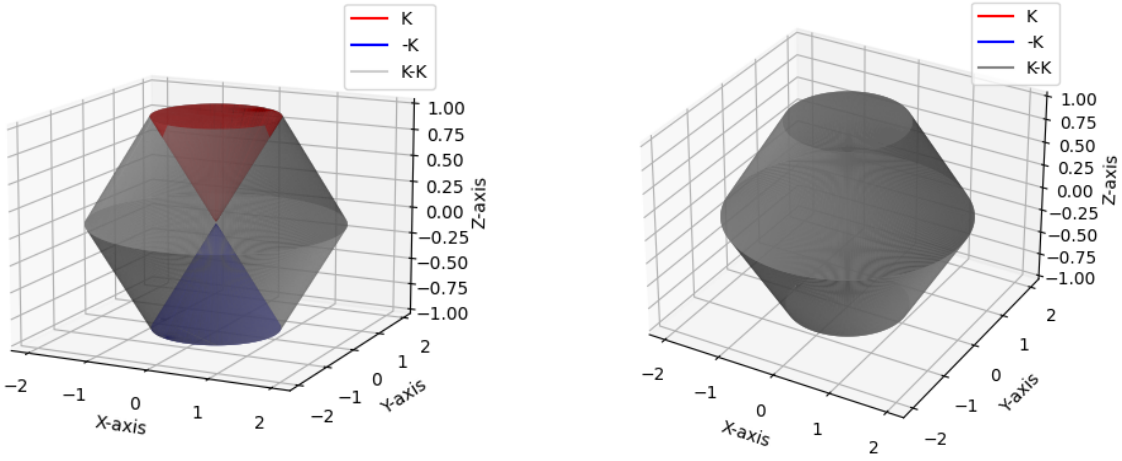

(a) View 1: K and $-K$ inside $K - K$ (b) View 2: $K - K$

Figure 3.10.1: Two different views of $K - K$ for the cone K

Again, we notice that if l goes to infinity, r behaves the same. Using the height h, we have that $l^2 = h^2 + r^2$, and by using h and r instead, we can take their individual limits to infinity since they are independent. This yields

$$\frac{S(K-K)}{S(K)} = \frac{6l + 2r}{r + l} = \frac{6\sqrt{h^2 + r^2} + 2r}{\sqrt{h^2 + r^2} + r}.$$

Then taking the limit with respect to r, then h, we obtain:

$$\lim_{r\to\infty} \frac{S(K-K)}{S(K)} = \lim_{r\to\infty} \frac{6\sqrt{h^2+r^2}+2r}{\sqrt{h^2+r^2}+r} = 4$$
$$\lim_{h\to\infty} \frac{S(K-K)}{S(K)} = \lim_{h\to\infty} \frac{6\sqrt{h^2+r^2}+2r}{\sqrt{h^2+r^2}+r} = 6.$$

Hence, the predicted upper bound C_K is reached when the cone's height tends to infinity. In that case, we have an infinite cone of radius r, and $K-K$ is comprised of two infinite cones connected by a circular base of radius $2r$. As for the limit when the radius tends to infinity, K's lateral faces collapse onto the circular base, and a second circular base is superposed on the original one. Hence, the Minkowski sum of a disk of radius r (which we have two of) with itself yields a disk of radius $2r$. Then the ratio of surface areas can be written as

$$\lim_{r\to\infty} \frac{S(K-K)}{S(K)} = \frac{2\pi r^2}{2(\pi(2r)^2)} = \frac{2\pi r^2}{4(2\pi r^2)} = 4.$$

Hence, cones behave like pyramids in terms of surface area, and this shows that in the particular case of pyramids, the ratio C_K for pyramids does not depend on the number of edges in $K's$ base, and this extends to cones when we take $m \to \infty$.

3.11 Randomly distributed vertices around a circular base: m_{even}.

Once the pattern for pyramids with a regular base was established, we moved on to the generalized pyramid. Using Python, we attempt to establish a trend in the formation of the difference body $K-K$, when K's base is no longer regular.

To obtain a noticeable pattern, we wrote a new Python code (see Appendix 3.3) that randomly distributes m vertices inside a circular base of radius R centered at

the origin, and the $(m+1)$'th vertex would be located at $(0,0,h)$ for some height h. The convex hull of these $m+1$ vertices would constitute K.

Initially, the vertices were chosen to be distributed in and around the circular base to promote K's random output, but was quickly dismissed when for larger m, some vertices became interior points when applying the *ConvexHull* function in Python. Hence, the code was changed to distribute the vertices around the perimeter of the circular base.

We also made sure that for the same m, as we increase h, the base remains the same randomly generated base, and as we increase r, the base is simply scaled to the new radius without modifying its shape. We will first deal with the numerical results before moving on to the geometric interpretation of $K - K$'s formation.

First, we deal with m_{even}, making sure to choose the same values for this section, namely $m = 4, 6, 10, 100$.

Table 3.11.1: Numerical results for $m = 4$

K_i	R	h	$S(K_i)$	$S(K_i - K_i)$	C_{K_i}
K_0	1	1	4.751	23.626	4.973
K_1	5	1	82.098	396.576	4.831
K_2	50	1	7931.255	38357.606	4.836
K_3	500	1	792818.339	3834360.084	4.836
K_4	10000	1	317126095.918	1533738384.015	4.436
K_5	1	5	14.999	84.018	5.601
K_6	1	50	134.592	801.249	5.953
K_7	1	500	1331.540	7982.899	5.995
K_8	1	10000	26600.642	159597.511	5.9998

Table 3.11.2: Numerical results for $m = 6$

L_i	R	h	$S(L_i)$	$S(L_i - L_i)$	C_{L_i}
L_0	1	1	6.064	28.471	4.695
L_1	5	1	118.118	527.626	4.467
L_2	50	1	11632.214	51816.570	4.455
L_3	500	1	1163038.948	5180699.296	4.454
L_4	10000	1	465214843.825	2072275857.932	4.454
L_5	1	5	17.128	93.829	5.478
L_6	1	50	148.517	881.833	5.938
L_7	1	500	1464.049	8774.991	5.994
L_8	1	10000	29236.740	175411.136	5.9997

Table 3.11.3: Numerical results for $m = 10$

A_i	R	h	$S(A_i)$	$S(A_i - A_i)$	C_{A_i}
A_0	1	1	6.583	29.736	4.517
A_1	5	1	131.976	555.709	4.211
A_2	50	1	13027.181	54611.056	4.192
A_3	500	1	1302545.414	5460134.131	4.192
A_4	10000	1	521017469.417	2184049736.828	4.192
A_5	1	5	17.828	96.719	5.425
A_6	1	50	152.585	905.108	5.932
A_7	1	500	1502.180	9002.659	5.993
A_8	1	10000	29994.050	179953.878	5.9997

Table 3.11.4: Numerical results for $m = 100$

B_i	R	h	$S(B_i)$	$S(B_i - B_i)$	C_{B_i}
B_0	1	1	7.568	32.889	4.346
B_1	5	1	158.195	636.355	4.023
B_2	50	1	15665.336	62711.283	4.003
B_3	500	1	1566377.894	6270194.966	4.003
B_4	10000	1	626550529.787	2508074224.218	4.003
B_5	1	5	19.139	102.308	5.345
B_6	1	50	160.133	948.267	5.922
B_7	1	500	1572.825	9424.422	5.992
B_8	1	10000	31396.925	188369.020	5.9996

We notice that contrarily to the evenly distributed m vertices around the base that we had earlier, for $C_{K_i}, C_{L_i}, C_{A_i}$, and C_{B_i}, where $0 \leq i \leq 4$, the constant does not approach the projected lower bound 4.0 as fast. It suffices to look at Table 3.8.1, where $C_{K_4} \approx 4.00000001$, while $C_{K_4} \approx 4.436$ in Table 3.11.1.

Since the vertices are no longer evenly distributed, the base of these bodies tends away from symmetry when m is small enough. This can be supported by the fact that the only time we are significantly approaching the lower bound is when $m = 100$. This is evident, since the increasing number of vertices around the base promotes an increasingly symmetric distribution, and B_i's base achieves a relatively balanced arrangement, which in turn affects the symmetry of its lateral faces. This emphasises the role of vertex density in shaping the overall symmetry characteristics of B_i's structure and its effect on $B_i - B_i$.

This phenomenon is evident in Figure 3.11.1, allowing for a direct comparison of the symmetry between $A_2 - A_2$ and $B_2 - B_2$. Upon inspecting the top base of

$A_2 - A_2$, which coincides with A_2's base, a notable asymmetry becomes apparent. Specifically, one of the vertices forms an almost right angle with its adjacent vertices. In contrast, when examining the base of $B_2 - B_2$, the nearly even distribution of vertices contributes to an appearance of near circularity.

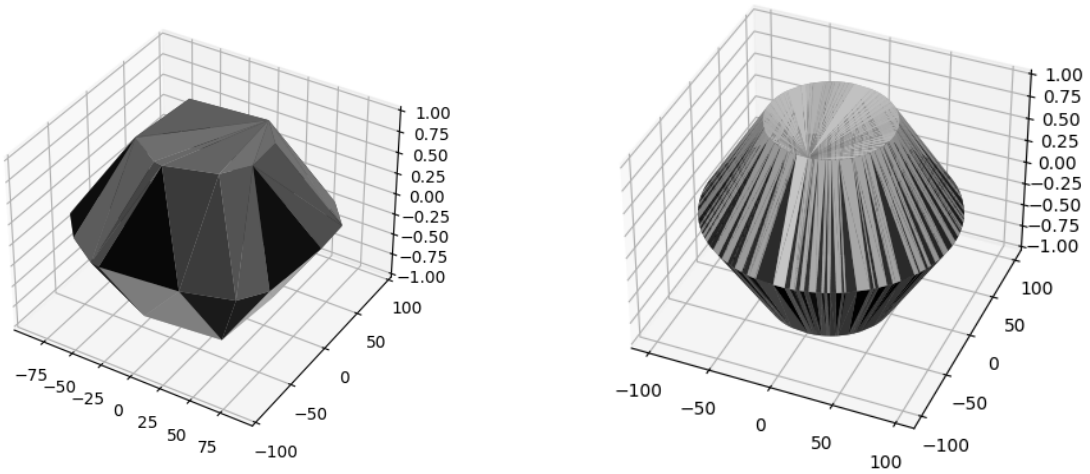

(a) $A_2 - A_2$ (b) $B_2 - B_2$

Figure 3.11.1: Difference in symmetry between $A_2 - A_2$ and $B_2 - B_2$

On the other hand, when we look at the constants for $5 \leq i \leq 8$, they seem to be behaving in the same manner that we've seen so far. When we compare evenly distributed and randomly distributed vertices, there is very little difference between the constants for the same m in Section 3.8. The bodies in both sections face no issues in approaching the upper bound as $h \to \infty$. This reinforces the importance of the base's symmetry in attaining the lower limit compared to the little impact it has on the upper bound due to the lack of discrepancy between these results.

3.12 Randomly distributed vertices around a circular base: m_{odd}.

We now deal with m_{odd}, and we choose the same constants $m = 3, 5, 7, 15, 105$ used in Section 3.9.

Table 3.12.1: Numerical results for $m = 3$

T_i	R	h	$S(T_i)$	$S(T_i - T_i)$	C_{T_i}
T_0	1	1	3.893	21.198	5.445
T_1	5	1	58.71	345.248	5.880
T_2	50	1	5558.277	33341.372	5.999
T_3	500	1	555481.582	3332881.186	5.99999
T_4	10000	1	222191236.190	1333147408.831	5.99999996
T_5	1	5	13.707	78.345	5.716
T_6	1	50	126.478	754.478	5.965
T_7	1	500	1254.719	7523.878	5.996
T_8	1	10000	25073.26	150435.170	5.9998

Table 3.12.2: Numerical results for $m = 5$

K_i	R	h	$S(K_i)$	$S(K_i - K_i)$	C_{K_i}
K_0	1	1	6.064	28.471	4.696
K_1	5	1	118.116	527.620	4.467
K_2	50	1	11631.940	51816.023	4.4546
K_3	500	1	1163011.564	5180644.528	4.4545
K_4	10000	1	465203890.123	2072253950.528	4.4545
K_5	1	5	17.128	93.829	5.478
K_6	1	50	148.516	881.829	5.938
K_7	1	500	1464.041	8774.945	5.994
K_8	1	10000	29236.588	175410.223	5.9997

Table 3.12.3: Numerical results for $m = 7$

L_i	R	h	$S(L_i)$	$S(L_i - L_i)$	C_{L_i}
L_0	1	1	6.288	29.019	4.615
L_1	5	1	124.102	539.740	4.349
L_2	50	1	12234.507	53021.307	4.334
L_3	500	1	1223272.361	5301166.273	4.334
L_4	10000	1	489308225.593	2120462621.619	4.334
L_5	1	5	17.430	95.075	5.455
L_6	1	50	150.269	891.855	5.935
L_7	1	500	1480.467	8873.017	5.993
L_8	1	10000	29562.811	177367.079	5.9997

Table 3.12.4: Numerical results for $m = 15$

A_i	R	h	$S(A_i)$	$S(A_i - A_i)$	C_{A_i}
A_0	1	1	6.880	30.675	4.459
A_1	5	1	139.900	579.575	4.143
A_2	50	1	13824.814	57007.594	4.124
A_3	500	1	1382314.094	5699798.597	4.123
A_4	10000	1	552924963.412	2279915566.246	4.123
A_5	1	5	18.227	98.422	5.400
A_6	1	50	154.898	918.339	5.929
A_7	1	500	1523.843	9132.003	5.993
A_8	1	10000	30424.289	182534.677	5.9996

Table 3.12.5: Numerical results for $m = 105$

B_i	R	h	$S(B_i)$	$S(B_i - B_i)$	C_{B_i}
B_0	1	1	7.568	32.900	4.346
B_1	5	1	158.203	636.374	4.023
B_2	50	1	15666.120	62713.215	4.003
B_3	500	1	1566456.258	6270388.192	4.003
B_4	10000	1	626581875.767	2508151514.816	4.003
B_5	1	5	19.140	102.309	5.345
B_6	1	50	160.135	948.279	5.922
B_7	1	500	1572.845	9424.540	5.992
B_8	1	10000	31397.317	188371.373	5.9996

So far, per the behaviour of C_K as $R \to \infty$, it would be expected that the constant would somehow decrease toward the lower bound. However, when comparing

the constants obtained for different m, we notice a big difference for the body $S, m = 3$. In Table 3.12.1, the constant C_{T_i} keeps increasing, while it decreases in the other tables for $0 \leq i \leq 4$. We can observe the same phenomenon in Section 3.7, where Table 3.7.1 also reveals that C_K is increasing alongside R. This is particular for $m = 3$, as for any other constant m, as $R \to \infty$, C_K is *decreasing*.

The Rogers-Shephard inequality (1.3) states that the equality case is reached when T is the simplex. In $\mathbb{R}^2$, we know that the Minkowski sum $T - T$ for a simplex T yields a body that is six times larger than T. Hence, if $R \to \infty$, T is now a triangular base, and $T - T$ is the Minkowski sum of the 2-dimensional simplices $\{T, -T\} \subset \mathbb{R}^3$. Furthermore, we shall not forget that once again, as $R \to \infty$, the lateral faces collapse onto the base, creating a second base on top of the first one. Since the base is no longer regular, we will denote the surface area of a triangle by $\frac{ab}{2}$, where b is the length of the base, and a is the height. Then by an elementary calculation, we get:

$$\lim_{R\to\infty} C_T = \lim_{R\to\infty} \frac{S(T-T)}{S(T)} = \frac{2(6(\frac{ab}{2}))}{2(\frac{ab}{2})} = 6$$

which explains the results obtained for $m = 3$.

For $m \neq 3$, the constants behave as expected; as R increases for $0 \leq i \leq 4$, $C_{K_i}, C_{L_i}, C_{A_i}$, and C_{B_i} are steadily decreasing towards 4.0, with the smallest constants for $i = 4$. Despite the lack of symmetry due to the odd number of vertices around the base accompanied by the randomization of their coordinates, these constants unsurprisingly remain tending towards the lower bound.

On the other end, when $R = 1$ and h increases, we see once again that $C_{K_i}, C_{L_i}, C_{A_i}$, and C_{B_i} are all increasing towards 6.0, nearing the upper bound as K tends towards an unbounded convex body.

3.13 Geometric interpretation of $K - K$'s formation

In previous sections, we explored the relationship between the dimensions of $K - K$ and K in various contexts. Now, we aim to synthesize these findings to discern a consistent pattern for the formation of $K - K$ in the context of pyramidal structures, as discussed in Section 3.6.

To begin, we must restate that $K - K$ consistently takes on the shape of two frustums of pyramids conjoined at their larger bases. Across all pyramidal structures, the smaller bases of these frustums correspond to the bases of K and $-K$.

When the vertices around the base are evenly distributed, as discussed in section 3.8, the scenario for m_{even} reveals that the lateral faces of $K - K$ consist of m_{even} isosceles trapezoids in each frustum. If K has a slant length of l and a base edge of s, these trapezoids have a height of l, a bottom base length of $2s$, and a top base length of s.

Alternatively, in the case of m_{odd} as detailed in Section 3.9, the lateral faces of $K - K$ comprise m_{odd} isosceles triangles in each frustum. Interestingly, these triangles coincide with the lateral faces of K and are interspersed with m_{odd} quadrilateral faces. The width of these triangles matches s, the base length of K, while their height is equivalent to c, the lateral edge of K.

In the scenario where m vertices are randomly distributed around the base, the configuration for m_{odd} remains consistent. In each frustum of $K - K$, we find m_{odd} triangular faces representing K's lateral faces, interspersed by m_{odd} quadrilaterals. Notably, in this context, we lose symmetry, as these faces are no longer congruent. This lack of symmetry becomes apparent in the top view, as illustrated in Figure 3.13.1.

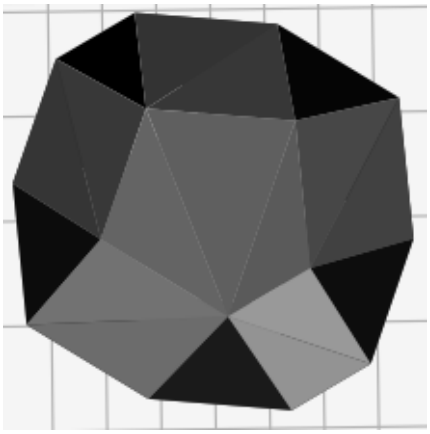

Figure 3.13.1: $K - K$: top view for $m = 5$ uniformly distributed vertices

In contrast, the configuration of $K - K$ for m_{even} differs. As observed previously, when these vertices are evenly distributed, the lateral faces of $K - K$ exhibit trapezoidal structures. However, in the absence of an even distribution, the trapezoidal formations dissipate. For a visual reference, consult Figure 3.13.2 with $m = 6$, offering a top view that facilitates observation of the upper frustum. The choice of a small vertex count aims to enhance visualization, allowing for generalization to all convex bodies K with randomly distributed vertices around the base for m_{odd}. It's crucial to note that the lower frustum mirrors the upper one, and the observations remain the same.

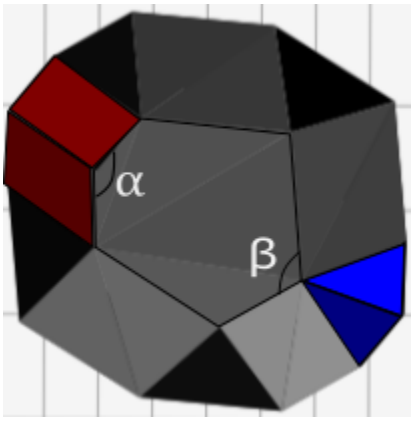

Figure 3.13.2: $K - K$: top view for $m = 6$ uniformly distributed vertices with angles α and β

To begin, we observe that each vertex around the base is connected to six triangular faces, which correspond to the lateral faces of K. Additionally, six quadrilateral faces are present, but their arrangement does not strictly separate the triangular faces. Indeed, originating from the edges connected by the angle α, we have two adjacent quadrilateral faces *(highlighted in red)*. Conversely, opposite to α, two adjacent triangular faces *(highlighted in blue)* emerge from the edges connected by the angle β. In essence, this occurs when there is an equal distribution of vertices on either side of α leading to β. Such a pattern is consistently observed in all convex bodies with m_{even} vertices around the base. However, it becomes progressively challenging to discern this pattern as m_{even} increases.

Clearly, despite the differences between the structures when K's base is regular and when it is not, the formation of $K - K$ can be generalized in the following way: if K is fixed and its base remains centered at the origin, if we move $-K$ about K to form $K - K$, then $K - K$ can be split into two equivalent parts by the plane of equation $z = h$. Each of these parts contains one copy of K's original faces, and m new quadrilateral faces that were formed during the process.

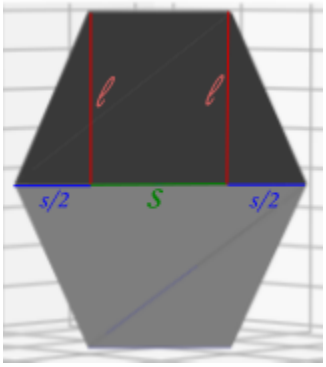

Figure 3.13.3: Dimensions of a trapezoidal face for $m = 4$

This observation extends even to the scenario of a regular base for m_{even}. Referring to Figure 3.13.3, as seen in Section 3.8, the isosceles trapezoids formed, characterized by a height l, bottom base length $2s$, and top base length s, result from

the lateral face of K splitting down the middle. This forms quadrilaterals with a width s and a length l, which emerge between the two halves of the triangles. Hence, we are also able to derive m quadrilateral faces and m triangular faces stemming from K in each frustum. Then if Q is the set of quadrilateral faces, we can summarise the ratio $S(K-K)$ as such:

$$S(K-K) = 2S(K) + S(Q)$$

where $2S(K) < S(Q) < 4S(K)$.

In the case of randomly distributed vertices, these quadrilateral faces are parallelograms. Then, if we let $\bar{c}$ and $\bar{s}$ be the largest lateral edge and base edge, respectively, then the area of the largest possible parallelogram P is

$$S(P) = |\vec{\bar{c}} \times \vec{\bar{s}}|.$$

Then by the same logic, the area of the largest lateral face in K is formed by the largest base edge and the largest lateral edge. Hence, since the lateral faces are triangles, the area of this largest lateral face T can be given by

$$S(T) = \frac{|\vec{\bar{c}} \times \vec{\bar{s}}|}{2}.$$

Now, in $K-K$, there are $2m$ parallelograms, and $2m$ triangular faces, as well as 2 bases. Using this, we can find a general equation for $S(K-K)$:

$$\begin{aligned} S(K-K) &= 2S(K) + S(Q) \\ &\leq 2S(K) + 2mS(P) \\ &= 2S(K) + 2m\ |\vec{c} \times \vec{s}|. \end{aligned}$$

Hence, the constant C_K can be generalized to:

$$\begin{aligned} C_K = \frac{S(K-K)}{S(K)} &= \frac{2S(K) + S(Q)}{S(K)} \\ &= 2 + \frac{S(Q)}{S(K)} \\ &= 2 + \frac{2}{S(K)} \sum_{i=1}^{m} S(P_i), \end{aligned}$$

where $P_i,\ 1 \leq i \leq m$, are the quadrilateral faces obtained in $K - K$

Addressing the ratio obtained above and achieving the optimal upper bound requires establishing a lower bound for $S(K)$. However, given our prior definition of $K - K$, selecting different edges for $S(K)$ is not feasible since $S(K - K)$ is directly contingent on $S(K)$. While opting for the largest base and lateral edges in our calculations could be a strategy, it compromises the established inequality. This approach essentially reduces the scenario to a pyramid with a regular base, where all edges are uniformly spaced and possess identical lengths, extending this property to all lateral edges as well. Consequently, choosing the maximum possible lengths for these edges merely returns us to previous cases, forcing us to maintain the same upper and lower bounds for C_K.

In conclusion, let s_i and l_i represent the respective lengths of a base edge and a slant edge forming a lateral face of K. For a convex body K with m vertices around the base, the total area of all lateral faces can be expressed as follows:

$$\sum_{i=1}^{m} \frac{s_i l_i}{2}.$$

Then, if B is K's base, this yields

$$\begin{aligned} S(K) =& S(B) + \sum_{i=1}^{m} \frac{s_i l_i}{2} \\ S(K - K) =& 2S(K) + S(Q), \end{aligned}$$

where $S(Q)$ represents the area of the quadrilateral faces. Thus, we have that $2S(K) < S(Q) < 4S(K)$.

These numerical findings for various convex bodies in $\mathbb{R}^3$ lead us to a significant conclusion, outlined in the following corollary, serving as a culmination of the deductions made following Theorem 2.3.1.

Corollary 3.13.1 For $n \geq 3$, the upper bound presented in Theorem 2.3.1 can be approached asymptotically. More precisely, this upper bound is achievable when one of K's vertices tends towards infinity.

We conjecture that the bound is obtained *only* asymptotically, which would follow from the completion of the claim in Section 2.3.

3.14 Bodies of revolution: The Reuleaux triangle.

The Reuleaux triangle is a planar convex body usually described as an equilateral triangle with rounded edges. Its boundary is composed of three circular arcs, all of the same radius, with centers at the end of the arcs. It is formed by the intersection of three disks, each with its center at the boundary of the other two. It is commonly known as the most famous non-circular body of constant width [5, p.106-110]. In other words, for all $u \in \mathbb{S}^{n-1}$,

$$w_K(u) = h_k(u) + h_K(-u) = \text{constant}.$$

We are interested in exploring the effect of the constant width property on the constant C_K by studying the constant for the body K taken to be the body of revolution of the Reuleaux triangle about the y-axis. By construction, this body of revolution which lies in $\mathbb{R}^3$ has constant width as well.

For some $r \in \mathbb{R}$, we begin with the Reuleaux triangle of width $w(u) = r$, where r is the radius of the disks that form it. Let its three vertices $A, B, C \in \mathbb{R}^2$ be:

$$A = \left(0, \frac{r}{\sqrt{3}}\right), \; B = \left(\frac{-r}{2}, \frac{-r}{2\sqrt{3}}\right), \; C = \left(\frac{r}{2}, \frac{-r}{2\sqrt{3}}\right).$$

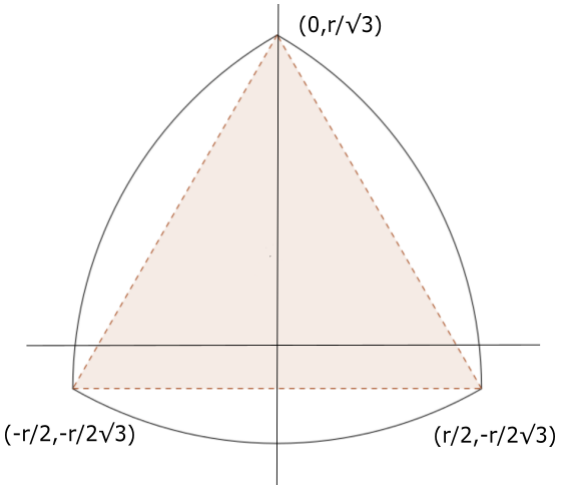

Figure 3.14.1: The Reuleaux triangle with width r

We can easily parametrize its boundary via the three disks that form it. We only need two curves: curve S connecting point B and point C, and curve R connecting point A and point C. Curve S is defined by the following equation:

$$x^2 + \left(y - \frac{r}{\sqrt{3}}\right)^2 = r^2.$$

While curve S is defined for $\frac{-r}{2} \leq x \leq \frac{r}{2}$, the body of revolution we are interested in is rotated about the y-axis, one of the axes of symmetry of the Reuleaux triangle positioned as above. Since the curve crosses the y-axis at the midpoint, we restrict it to $0 \leq x \leq \frac{r}{2}$. We can now define the following parametrization:

$$x_1(\theta) = r\cos\theta, \qquad y_1(\theta) = r\sin\theta + \frac{r}{\sqrt{3}} \qquad \text{for } -\tfrac{\pi}{2} \leq \theta \leq -\tfrac{\pi}{3}.$$

Curve R is defined as

$$\left(x + \frac{r}{2}\right)^2 + \left(y + \frac{r}{2\sqrt{3}}\right)^2 = r^2$$

and has parametrization

$$x_2(\theta) = r\cos\theta - \frac{r}{2}, \qquad y_2(\theta) = r\sin\theta - \frac{r}{2\sqrt{3}} \qquad \text{for } 0 \leq \theta \leq \tfrac{\pi}{3}.$$

Then K is formed by rotating these two curves about the y-axis. Since we are interested in the surface area of K, we can use the well-known formula for the surface area of a body of revolution:

Lemma 3.14.1 Let A be a body of revolution generated by a parametric curve $(x(\theta), y(\theta)) \in \mathbb{R}^2$ defined for $\theta \in D = [a, b]$. If the curve is revolved around the $y-$axis, then the surface area of A is given by

$$S(A) = 2\pi \int_D x(\theta)\sqrt{(x'(\theta))^2 + (y'(\theta))^2}d\theta.$$

Then, using this formula, we can easily calculate the surface area obtained by revolving the Reuleaux triangle about the y-axis:

$$\begin{aligned}
S(K) =& 2\pi \int_{\frac{-\pi}{2}}^{\frac{-\pi}{3}} x_1(\theta)\sqrt{(x_1'(\theta))^2 + (y_1'(\theta))^2}\, d\theta + 2\pi \int_0^{\frac{\pi}{3}} x_2(\theta)\sqrt{(x_2'(\theta))^2 + (y_2'(\theta))^2}\, d\theta \\
=& 2\pi \int_{\frac{-\pi}{2}}^{\frac{-\pi}{3}} r\cos\theta\sqrt{(-r\sin\theta)^2 + (r\cos\theta)^2}\, d\theta + \int_0^{\frac{\pi}{3}} (r\cos\theta - \frac{r}{2})\sqrt{(-r\sin\theta)^2 + (r\cos\theta)^2}\, d\theta \\
=& 2\pi \int_{\frac{-\pi}{2}}^{\frac{-\pi}{3}} r^2\cos\theta\, d\theta + 2\pi \int_0^{\frac{\pi}{3}} (r^2\cos\theta - \frac{r^2}{2})\, d\theta \\
=& 2\pi r^2 \sin\theta\Big|_{\frac{-\pi}{2}}^{\frac{-\pi}{3}} + 2\pi(r^2\sin\theta - \frac{\theta r^2}{2})\Big|_0^{\frac{\pi}{3}} \\
=& 2\pi r^2(-\frac{\sqrt{3}}{2} + 1) + 2\pi r^2(\frac{\sqrt{3}}{2} - \frac{\pi}{6}) \\
=& 2\pi r^2(1 - \frac{\pi}{6}).
\end{aligned}$$

To find the area for the difference body $K - K$, we first need to consider some properties of the body of revolution K we have obtained. We have purposely chosen to perform the rotation of the Reuleaux triangle with constant width $w(u) = r$ about one of its axes of symmetry to obtain a body K that also has constant width $w_K(u) = r$ [7, p. 171-172]. Since the support function of the Minkoswki sum of convex bodies is the sum of support functions of the bodies being added, we have that

$$\begin{aligned}
w_{K-K}(u) =& h_{K-K}(u) + h_{K-K}(-u) \\
=& h_K(u) + h_{-K}(u) + h_K(-u) + h_{-K}(-u) \\
=& h_K(u) + h_K(-u) + h_{-K}(u) + h_{-K}(-u) \\
=& w_K(u) + w_{-K}(u).
\end{aligned}$$

Hence, we have that $w_{K-K}(u) = 2r$. Furthermore, $K - K$ is the Minkowski sum of two bodies of constant width r, and it is known that $K - K$ is a ball if and only if K has constant width [1]. Hence, $K - K$ is a ball of radius $2r$, which yields:

$$S(K - K) = 2\pi(2r)^2 = 4\pi R^2.$$

Combining these results, we obtain the following constant:

$$\begin{aligned} C_K =& \frac{S(K-K)}{S(K)} \\ =& \frac{4\pi r^2}{2\pi r^2(1-\frac{\pi}{6})} \\ =& \frac{2}{(1-\frac{\pi}{6})} \\ \approx& 4.198. \end{aligned}$$

Despite its asymmetry, the associated constant for the Reuleaux body is notably close to that of a symmetric convex body K. This proximity suggests that the Minkowski sum of the Reuleaux body of revolution being a ball, and thus centrally symmetric, significantly influences the closeness of this constant to the established lower bound.

The intriguing nature of these findings stems from the non-symmetric characteristics of the Reuleaux body of revolution, parameterized by r. Despite its lack of symmetry, a quantifiable measure of its geometric dissimilarity arises through the *Hausdorff distance*. This distance, defined between any two non-empty compacts sets $K, L \subset \mathbb{R}^n$, is given by:

$$d_{\mathcal{H}}(K, L) := \inf\{\lambda \geq 0 : K \subseteq L + \lambda B^n \text{ and } L \subseteq K + \lambda B^n\},$$

where B^n is the closed unit ball in $\mathbb{R}^n$. Equivalently, it can also be described as

$$d_{\mathcal{H}}(K,L) := \max\left\{\sup_{x\in K} \operatorname{dist}(x,L), \sup_{y\in L} \operatorname{dist}(y,K)\right\}.$$

Furthermore, this definition can be specified to *convex*, compact and non-empty sets $K_1, K_2 \subset \mathbb{R}^n$ as such:

$$d_{\mathcal{H}}(K_1,K_2) := \max\{|h_{K_1}(u) - h_{K_2}(u)| : u \in \mathbb{S}^{n-1}\},$$

where h_{K_1} and h_{K_2} are the support functions of K_1 and K_2, respectively.

If one takes an infimum of the Hausdorff distance between K_1 and K_2 after all translations of one of the sets, say K_2, this is a measure of how different the two sets are, and this is the sense in which the Hausdorff distance is generally used. As such, the Hausdorff distance of the Reuleaux body of revolution of width r from a cone obtained by rotating the regular 2-dimensional simplex of side length r about one of its altitudes is precisely $r(1-\sqrt{3}/2)$. Surprisingly, despite its lack of symmetry, the calculations above show that the associated constant for the Reuleaux body of revolution is relatively close to that of a symmetric convex body K.

This observation prompts a deeper consideration of the stability associated with the surface area inequality of the difference body. The proximity of the constant obtained for the Reuleaux body of revolution and that of a symmetric body suggests that there may not be a stability result associated to the inequality for the surface area of the difference body, in contrast to the classical Rogers-Shephard inequality, (1.3), for which stability results have been established, [4]. In the context of stability, C_{K_1} and C_{K_2} attaining close values should imply that K_1 and K_2 are convex bodies that are close within the Hausdorff metric.

Appendix

Listing 3.1: Python code for the regular simplex

```
import math
import matplotlib.pyplot as plt
import matplotlib.patches as mpatches
import numpy as np
from scipy.spatial import ConvexHull


k = np.array([(0, 0, 0), (1/math.sqrt(2), 0, 1/math.sqrt(2)),
   (0, 1/math.sqrt(2), 1/math.sqrt(2)), (1/math.sqrt(2), 1/
   math.sqrt(2), 0)])
v = np.array(-k)
minkowski_sum = k[:, None, :] + v[None, :, :]
minkowski_sum = minkowski_sum.reshape(-1, 3)
hull = ConvexHull(minkowski_sum)
D = minkowski_sum[hull.vertices]
k_hull = ConvexHull(k)
k_area = k_hull.area
D_hull = ConvexHull(D)
D_area = D_hull.area


print("Vertices␣of␣k:␣\n", k)
print("Vertices␣of␣-k:␣\n", -k)
```

```
print("Vertices␣of␣the␣convex␣hull␣of␣the␣Minkowski␣sum:␣\n",
   D)
print("Surface␣area␣of␣the␣original␣set␣of␣vertices:␣", k_area
   )
print("Surface␣area␣of␣the␣convex␣hull␣of␣the␣Minkowski␣sum:␣"
   , D_area)
print("Surface␣area␣of␣the␣convex␣hull␣of␣the␣Minkowski␣sum:␣"
   , D_area / k_area, "␣times␣the␣surface␣area␣of␣k")


fig = plt.figure()
ax = fig.add_subplot(111, projection='3d')
ax.plot_trisurf(k[:, 0], k[:, 1], k[:, 2], triangles=k_hull.
   simplices, color='red', alpha=0.5, label='k')
ax.plot_trisurf(-k[:, 0], -k[:, 1], -k[:, 2], triangles=k_hull
   .simplices, color='blue', alpha=0.5, label='-k')
ax.plot_trisurf(D[:, 0], D[:, 1], D[:, 2], triangles=D_hull.
   simplices, color='grey', alpha=0.6, label='Minkowski␣Sum')
ax.set_xlim([-1, 1])
ax.set_ylim([-1, 1])
ax.set_zlim([-1, 1])
ax.set_xlabel('X')
ax.set_ylabel('Y')
ax.set_zlabel('Z')
legend_handles = [
    plt.Line2D([0], [0], linestyle='-', color='red'),
    plt.Line2D([0], [0], linestyle='-', color='blue'),
    mpatches.Patch(facecolor='grey', alpha=1),
    plt.Line2D([0], [0], linestyle='-', color='black')
]
```

```
legend_labels = ['k', '-k', 'Minkowski␣Sum']
ax.legend(legend_handles, legend_labels)
plt.show()
```

Listing 3.2: Python code for evenly distributed vertices around the base

```
import math
import matplotlib.pyplot as plt
import numpy as np
from scipy.spatial import ConvexHull


m = 6
r = 1
h = 1



def main(plot_option):
    theta = np.linspace(0, 2 * math.pi, m + 1)[:-1]
    x = r * np.cos(theta)
    y = r * np.sin(theta)
    z = np.ones_like(x) * h
    v = np.vstack((x, y, z)).T
    v = np.vstack((v, np.array([0, 0, 0])))
    k = v
    w = -v
    minkowski_sum = k[:, None, :] + w[None, :, :]
    minkowski_sum = minkowski_sum.reshape(-1, 3)
    hull = ConvexHull(minkowski_sum)
    d = minkowski_sum[hull.vertices]
    print("Vertices␣of␣K-K:␣\n", d)
    print("Vertices␣of␣K:␣\n", k)
    print("Vertices␣of␣-K:␣\n", w)
    k_hull = ConvexHull(k)
    k_area = k_hull.area
```

```
print("Surface␣area␣of␣K:␣", k_area)
D_hull = ConvexHull(d)
D_area = D_hull.area
print("Surface␣area␣of␣K-K:␣", D_area)
print("Surface␣area␣of␣K-K␣/␣Surface␣area␣of␣K:␣", D_area
   / k_area)

if plot_option:
    fig = plt.figure()
    ax = fig.add_subplot(111, projection='3d')

    ax.plot_trisurf(k[:, 0], k[:, 1], k[:, 2], triangles=
       k_hull.simplices, color='red', alpha=0.4, label='K'
       )
    ax.plot_trisurf(w[:, 0], w[:, 1], w[:, 2], triangles=
       k_hull.simplices, color='blue', alpha=0.4, label='-
       K')

    for i, simplex in enumerate(D_hull.simplices):
        if any(vertex == len(k) for vertex in simplex):
            ax.plot_trisurf(d[simplex, 0], d[simplex, 1],
               d[simplex, 2], color='grey', alpha=1, label
               ='K-K')
        else:
            ax.plot_trisurf(d[simplex, 0], d[simplex, 1],
               d[simplex, 2], color='grey', alpha=1)

    ax.set_xlabel('X-axis')
    ax.set_ylabel('Y-axis')
```

```
        ax.set_zlabel('Z-axis')

        ax.legend(handles=[plt.Line2D([0], [0], color='red',
           label='K'),
                           plt.Line2D([0], [0], color='blue',
                              label='-K'),
                           plt.Line2D([0], [0], color='grey',
                              alpha=1, label='K-K')])

        plt.show()


if __name__ == '__main__':
    main(plot_option=True)
```

Listing 3.3: Python code for randomly distributed vertices around the base

```
import math
import numpy as np
import matplotlib.pyplot as plt
from scipy.spatial import ConvexHull
from mpl_toolkits.mplot3d import Axes3D


m = 100
r = 50
h = 1



def main(plot_option):
    np.random.seed(42)
    theta = np.random.uniform(0, 2 * math.pi, m)
    x = r * np.cos(theta)
    y = r * np.sin(theta)
    z = np.ones_like(x) * h
    v = np.vstack((x, y, z)).T
    v = np.vstack((v, np.array([0, 0, 0])))


    print("Vertices␣of␣the␣original␣set␣of␣vertices:␣\n", v)


    k = v
    w = -v
    minkowski_sum = k[:, None, :] + w[None, :, :]


    minkowski_sum = minkowski_sum.reshape(-1, 3)
    hull = ConvexHull(minkowski_sum)
```

```
d = minkowski_sum[hull.vertices]
print("Vertices␣of␣the␣convex␣hull␣of␣the␣Minkowski␣sum:␣\
   n", d)
k_hull = ConvexHull(k)
k_area = k_hull.area
print("Surface␣area␣of␣the␣original␣set␣of␣vertices:␣",
   k_area)
D_hull = ConvexHull(d)
D_area = D_hull.area
print("Surface␣area␣of␣the␣convex␣hull␣of␣the␣Minkowski␣
   sum:␣", D_area)
print("Surface␣area␣of␣the␣convex␣hull␣of␣the␣Minkowski␣
   sum:␣", D_area / k_area, "␣times␣the␣surface␣area␣of␣k"
   )

if plot_option:
    fig = plt.figure()
    ax = fig.add_subplot(111, projection='3d')
    ax.plot_trisurf(k[:, 0], k[:, 1], k[:, 2], triangles=
       k_hull.simplices, color='red', alpha=0)

    face_colors = plt.cm.gray(np.linspace(0, 1, len(D_hull
       .simplices)))

    for i, simplex in enumerate(D_hull.simplices):
        ax.plot_trisurf(d[simplex, 0], d[simplex, 1], d[
           simplex, 2], color=face_colors[i], alpha=1)

    plt.show()
```

```
if __name__ == '__main__':
    main(plot_option=True)
```

Python Code Output

Listing 3.4: Python code output for the regular simplex

```
Vertices of k:
[[0.          0.          0.        ]
 [0.70710678 0.          0.70710678]
 [0.          0.70710678 0.70710678]
 [0.70710678 0.70710678 0.        ]]
Vertices of -k:
[[-0.          -0.          -0.        ]
 [-0.70710678 -0.          -0.70710678]
 [-0.          -0.70710678 -0.70710678]
 [-0.70710678 -0.70710678 -0.        ]]
Vertices of the convex hull of the Minkowski sum:
[[-0.70710678  0.          -0.70710678]
 [ 0.          -0.70710678 -0.70710678]
 [-0.70710678 -0.70710678  0.        ]
 [ 0.70710678  0.           0.70710678]
 [ 0.70710678 -0.70710678  0.        ]
 [ 0.          -0.70710678  0.70710678]
 [ 0.           0.70710678  0.70710678]
 [-0.70710678  0.70710678  0.        ]
 [-0.70710678  0.           0.70710678]
 [ 0.70710678  0.70710678  0.        ]
 [ 0.           0.70710678 -0.70710678]
 [ 0.70710678  0.          -0.70710678]]
Surface area of the original set of vertices:
   1.7320508075688767
```

```
Surface area of the convex hull of the Minkowski sum:
   9.464101615137753
Surface area of the convex hull of the Minkowski sum:
   5.464101615137755 times the surface area of k
```

Bibliography

[1] Judit Abardia and Eugènia Saorin Gómez, *How do difference bodies in complex vector spaces look like? A geometrical approach*, Communications in Contemporary Mathematics, 2015, 17(04), 1450023. DOI: 10.1142/s0219199714500230

[2] Vitor Balestro, Horst Martini, and Ralph Teixeira, *Convexity From the Geometric Point of View*, Birkhäuser, 2024.

[3] Vladimir Grigorevich Boltyanski and Jesús Jerónimo Castro, *Centrally Symmetric Convex Sets*, Journal of Convex Analysis 2007, 14 (2), 345-351.

[4] Károly Böröczky, *The Stability of the Rogers-Shephard Inequality and of Some Related Inequalities*, Advances in Mathematics, 2005, 190(1), 47-76. DOI: 10.1016/j.aim.2003.11.015

[5] Richard John Gardner, *Geometric Tomography*, 2nd ed., Encyclopedia of Mathematics and its Applications, Cambridge University Press, 2006.

[6] Peter Manfred Gruber, *Convex and Discrete Geometry*, Springer Science & Business Media, 2007.

[7] Horst Martini, Luis Montejano, and Déborah Oliveros, *Bodies of Constant Width: An Introduction to Convex Geometry with Applications*, 1st ed. Birkhäuser Cham, 2019.

[8] Fadia Ounissi, *Rogers-Shephard type inequalities and upper bounds for mixed volumes of a cube gradually reduced to a simplex in* $\mathbb{R}^3$, Unpublished undergraduate honours project, Concordia University, 2021.

[9] Claude Ambrose Rogers and Geoffrey Colin Shephard, *The difference body of a convex body*, Arch. Math, 1957, 8, 220-233. DOI: 10.1007/BF01899997

[10] Rolf Schneider, *Convex Bodies: The Brunn-Minkowski Theory*, 2nd ed. Cambridge University Press, 2014.

[11] Gábor Tóth, *Measures of Symmetry for Convex Sets and Stability*, Universitext, Springer, Cham, 2015. DOI: 10.1007/978-3-319-23733-6

[12] Martin Winter, *Maximum vertex amount of low-dimensional simplex projection*, MathOverflow, https://mathoverflow.net/q/407161, (Version: 2021-10-28).